Journal Pre-proofs

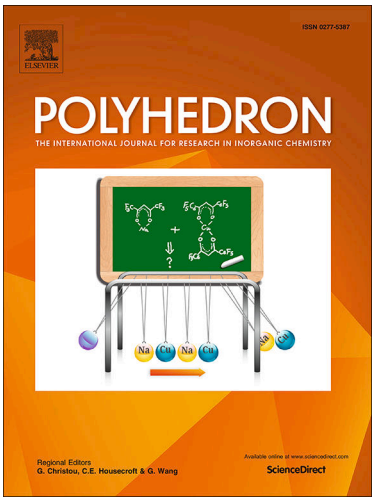

An oxalate-bridged oxidovanadium(iv) binuclear complex that improves the *in vitro* cell uptake of a fluorescent glucose analog

Gabriel B. Baptistella, Graciele C.M. Manica, Susan W. de Souza, Francielli S. Santana, Lucas G. Fachini, David L. Hughes, Eduardo Lemos de Sá, Geraldo Picheth, Jaísa F. Soares, Fabiane G. De M. Rego, Giovana G. Nunes

PII: S0277-5387(21)00053-X
DOI: https://doi.org/10.1016/j.poly.2021.115071
Reference: POLY 115071

To appear in: *Polyhedron*

Received Date: 7 August 2020
Revised Date: 21 December 2020
Accepted Date: 26 January 2021

Please cite this article as: G.B. Baptistella, G.C.M. Manica, S.W. de Souza, F.S. Santana, L.G. Fachini, D.L. Hughes, E. Lemos de Sá, G. Picheth, J.F. Soares, F.G. De M. Rego, G.G. Nunes, An oxalate-bridged oxidovanadium(iv) binuclear complex that improves the *in vitro* cell uptake of a fluorescent glucose analog, *Polyhedron* (2021), doi: https://doi.org/10.1016/j.poly.2021.115071

AN OXALATE-BRIDGED OXIDOVANADIUM(IV) BINUCLEAR COMPLEX THAT IMPROVES THE *IN VITRO* CELL UPTAKE OF A FLUORESCENT GLUCOSE ANALOG

Gabriel B. Baptistella[1], Graciele C. M. Manica[2], Susan W. de Souza[2], Francielli S. Santana[1], Lucas G. Fachini[1], David L. Hughes[3], Eduardo Lemos de Sá[1], Geraldo Picheth[2], Jaísa F. Soares[1], Fabiane G. de M. Rego[2], Giovana G. Nunes[1*]

[1]*Departamento de Química, Universidade Federal do Paraná, Centro Politécnico, Jardim das Américas, 81530-900 Curitiba, Paraná, PR, Brazil*

[2]*Programa de Pós-graduação em Ciências Farmacêuticas, Universidade Federal do Paraná, Curitiba, PR, Brazil*

[3]*School of Chemistry, University of East Anglia, Norwich, NR4 7TJ, United Kingdom*

Correspondence to Giovana G. Nunes (e-mail: nunesgg@ufpr.br)

Graphical abstract

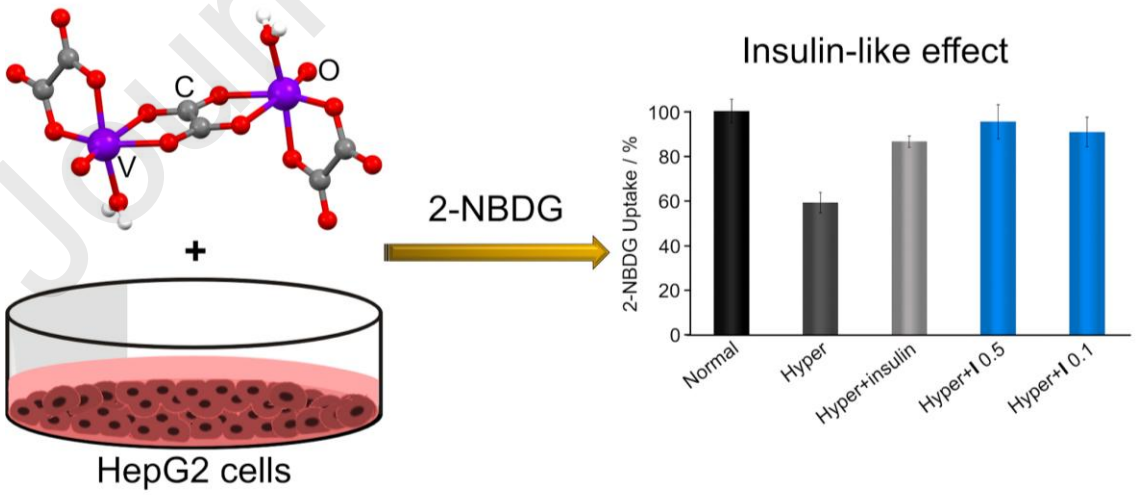

Abstract

The centrosymmetric oxidovanadium(IV) complex $(Et_3NH)_2[\{VO(OH_2)(ox)\}_2(\mu\text{-}ox)]$ (**I**), where ox^{2-} = oxalate, was synthesized and characterized by X-ray diffraction (single-crystal and powder, PXRD), thermogravimetric (TGA), magnetic susceptibility (at room temperature) and spectroscopic analyses (infrared, Raman and electron paramagnetic resonance, EPR, spectroscopies). In the solid state, each vanadium center is coordinated by the oxygen atoms of a bis-bidentate oxalate bridging ligand, a terminal oxalate, an oxo group and one water molecule. The electronic structure of the binuclear complex was investigated by density functional theory (DFT) calculations, both in vacuum and in a simulated aqueous environment, employing the ωB97XD functional and the def2TZVP basis set. The cytotoxicity of **I** was evaluated *in vitro* in the human hepatocellular carcinoma cell line HepG2, giving an IC_{50} value of 15.67 μmol L^{-1} after incubation for 24 h. The EPR analysis of **I** in aqueous solution suggested the maintenance of the binuclear structure, while in the hyperglycemic medium DMEM the complex suffers dissociation to give a mononuclear oxidovanadium(IV) species. HepG2 cell treatment with 0.10 and 0.50 μmol L^{-1} of **I** in DMEM increased 2-NBDG (2-[*N*-(7-nitrobenz-2-oxa-1,3-diazol-4-yl)amino]-2-deoxy-D-glucose) uptake significantly (up to 91% as compared to HepG2 in hyperglycemic condition, 59 %). These results indicate a promising activity of **I** to be investigated further in additional antidiabetic studies.

Keywords: oxidovanadium(IV); oxalate; 2-NBDG uptake; HepG2 cells; crystal structure analysis.

1. INTRODUCTION

Vanadium(IV)/(V) compounds have gained attention in drug development due to their insulin-like, anti-diabetic, anti-cancer and anti-microbial activities [1, 2]. As far as the potential anti-diabetic role of vanadium-containing species is concerned, studies in rodent models of type 1 and type 2 diabetes mellitus have shown that vanadium compounds influence the insulin signaling pathway [3]. Despite these promising *in vivo* results, the well-known bis(ethylmaltolato)oxidovanadium(IV) (BEOV) complex, first synthesized in the late 1990s, is the only coordination compound of vanadium for which the phase IIa of clinical trials in humans was completed [4]. More recently, a case study with a Chinese population demonstrated that plasma levels of vanadium and type 2 diabetes were inversely related, meaning that individuals with higher plasma vanadium concentrations were significantly less likely to develop the disease [5].

A wide range of coordination compounds of vanadium act as insulin-mimetics [3, 6]. For instance, oxidovanadium(IV/V) chlorodipicolinate species improve hyperglicemia and glucose intolerance in streptozotocin (STZ)-induced diabetic rats [7]. Also, $VOSO_4$ was shown to improve glucose uptake in human hepatocellular carcinoma (HepG2) cells via a signaling pathway activated by generation of the $^{\bullet}OH$ radical, which has a key role in the insulin receptor/protein kinase B phosphorylation system [8]. In this context, HepG2 cells are considered an alternative for *in vitro* investigation of insulin-dependent pathways, due to the conservation of characteristics common to hepatocytes and preservation of the glucose transporter (GLUT) activity [9-11].

Studies performed in the intestinal tract, blood, and mammalian cells suggest that vanadium species undergo redox reactions and ligand exchange processes in both blood plasma and intracellular fluid. The most likely active insulin-mimetic species, the $H_2VO_4^-$ anion, inhibits the tyrosine phosphatase 1B (PTPase 1B) enzyme. This action prevents the dephosphorylation of the insulin receptor's intracellular tyrosine, enhances the activity of the insulin receptor's kinase (and other kinases in the signaling path), and recovers glucose uptake [12].

In the coordination chemistry of transition metals such as vanadium, much attention has been devoted to oxalate-containing ($C_2O_4^{2-}$ or ox^{2-}) complexes due to their interesting structural, catalytic [13, 14] and magnetic features.[15, 16]. The bioinorganic relevance of vanadium-oxalate chemistry, in its turn, has been addressed in a variety of levels [16-18]. Under physiological conditions, vanadium(IV) has a high affinity for *O*-donor bioligands as lactate, citrate and oxalate, which prevents hydrolysis and precipitation of insoluble $VO(OH)_2$ [19]. The potential therapeutic action of well-characterized, water-soluble vanadium oxalate compounds, on the other hand, remains much less explored.

Over the last decade, some of us have been investigating the electronic, magnetic and pharmacological properties of different classes of vanadium compounds [20-23]. This work reports the preparation, structural characterization, DFT studies and solution behavior of the binuclear, oxalate-bridged oxidovanadium(IV) $[\{VO(OH_2)(ox)\}_2(\mu\text{-}ox)]^{2-}$ complex (**I**). Toxicity essays with **I** and HepG2 cells shed light on the range of concentrations that can be employed in insulin-mimetic investigations. We show that the 2-NBDG ((2-[*N*-(7-nitrobenz-2-oxa-1,3-diazol-4-yl)amino]-2-deoxy-D-glucose)) uptake by HepG2 cells treated with solutions of **I** in culture medium DMEM was similar or better than that observed in the presence of insulin in hyperglycemic condition. These findings suggest a

potentially relevant role not only of **I** but also of other biologically-formed oxalate complexes, pointing to a vanadium-related anti-diabetic activity.

2. EXPERIMENTAL

2.1. Materials and methods

2.1.1. Solutions, chemicals and biochemicals

All reactants and solvents were employed as acquired. Sigma-Aldrich supplied vanadium pentoxide (V_2O_5, 99.6%), triethylamine (Et_3N, 99%) and 1,3-butanediol (1,3-bd, >98%), while oxalic acid ($H_2C_2O_4{\cdot}2H_2O$, 97%) was purchased from Ecibra. The synthesis of **I** was carried out in ultrapure water (Milli-Q, Millipore type 1, resistivity of 18.2 MΩ·cm at 25 °C). The materials used in the biological assays were sterilized in a Tuttnauer autoclave (model 3150EL). The cell cultures were incubated in a humidified LOBOV CientificaTM incubator at 37 ºC in 5% CO_2. The Dulbelco DMEM culture medium (Dulbecco modification of Minimum Essential Media, Gibco), phosphate-saline buffer (PBS, Prolab), gentamicin (Novafarma), fetal bovine serum (FBS, Gibco), 2-(*N*-(7-nitrobenz-2-oxa-1,3-diazol-4-yl)amino)-2-deoxy-D-glucose (2-NBDG, Invitrogen), MTT cell proliferation assay kit (VWR), and D-(+)-glucose (> 99%, Aldrich) were also used without further purification.

2.1.2. Analytical methods and instruments

Carbon, hydrogen and nitrogen contents were determined by combustion in a Perkin Elmer 2400 Series II Elemental Analyzer. Vanadium contents were determined on an Opkin Elmer Optima 8300 series atomic emission spectrometer with inductively-coupled plasma (ICP-OES). The X-ray powder diffraction (PXRD) pattern of **I** was recorded at 40 kV and 40 mA on a Shimadzu XRD-600 diffractometer equipped with a Cu-target tube (Cu-K_α, λ = 1.5418 Å). The 2θ range of 5–50° was employed in the measurements. The calculated diffractogram of **I**, in turn, was generated from the single-crystal crystallographic information (CIF) file using the Mercury 4.0 software [24]. Infrared (IR) data were recorded from KBr pellets on a BOMEM MB100 FIT-IR spectrophotometer with a resolution of 4 cm^{-1} in the 400–4000 cm^{-1} range. Raman spectra were obtained on a Raman Confocal Witec alpha 300R microscope, with a He–Ne (632.8nm) laser and a resolution of 0.02 cm^{-1}. The electronic spectra were registered on a PerkinElmer Lambda 1050 UV-Vis-NIR spectrophotometer. Continuous-Wave (CW) X-band EPR spectra (9.5 GHz) were recorded on powdered solid samples and in aqueous solution at room temperature and 77 K, using a Bruker EMX-micro spectrometer. Thermogravimetric analyses (TGA) were run on a Netzsch STA449 F3 Jupiter analyzer instrument equipped with a silicon carbide furnace and using N_2/O_2 as carrier gas. Samples (*ca.* 4.0 mg) were heated in aluminum pans from 100 °C to 700 °C at 10 °C min^{-1}. Magnetic susceptibility measurements were performed in the solid state at room temperature (297 K) on a MKII magnetic susceptibility balance from Johnson-Matthey, using a modified Gouy method [25]. Pascal constants were employed to correct the experimental values for the diamagnetism of the ligands and the paired electrons on the metal [26].

*2.1.3. Synthesis of complex **I***

A dark yellow suspension of V_2O_5 (0.400 g, 2.20 mmol) in 7.0 mL of water received the addition of 0.830 g of $H_2C_2O_4{\cdot}2H_2O$ (6.60 mmol). The reaction mixture was stirred at 60 °C for 2 h, producing a dark blue solution to which 200 µL of 1,3-*bd* (2.20 mmol) in 260 µL of ethyl alcohol (2.21 mmol) and 610 µL (4.39 mmol) of Et_3N were added. After two more hours, the resulting dark green solution was filtered and poured into a Petri dish. Light greenish-blue crystals were formed after 24 h and the supernatant was removed; the crystals were washed with 3 x 5.0 mL of ethyl alcohol and finally dried in the air to render 0.833 g of **I**. Yield: 63% based on vanadium. The product was highly soluble in water (100 mg mL^{-1}). Elemental analysis calculated (%) for $C_{18}H_{36}O_{16}N_2V_2$ (638.37 g mol^{-1}): V, 15.96; C, 33.86; H, 5.68; N, 4.38; found: V, 15.06; C, 33.96; H, 5.66; N, 4.33%. FTIR (KBr, cm^{-1}, s = strong, m = medium, w = weak, br = broad): 3415(b), 1691(m), 1637(m), 1400(s), 1263(s), 1161(w), 989(s), 811(s), 549(m), 489(m). TG analysis (Fig. S1) provided the following weight losses: *(i)* from 150 to 290 °C, corresponding to the two Et_3NH^+ and two H_2O molecules (calculated 37.6%; found 37.9%); *(ii)* from 290 to 485 °C, related to the two terminal oxalate ligands (calculated 27.6%; found 28.05%); *(iii)* up to 485 °C, bridging oxalate (calculated 13.9%; found 13.8%).

2.2. Single-crystal X-ray structural analysis

A greenish-blue crystal of **I** (0.207 x 0.109 x 0.073 mm^3) was mounted on a MiTeGen® micromesh. The diffraction data were measured at 300(2) K on a Bruker D8 Venture diffractometer equipped with a Photon 100 CMOS detector, Mo–Kα radiation (0.71073 Å) and graphite monochromator. Data were processed using the APEX3 program [27]. The structure was determined by dual methods in the SHELXT software [28] and refined by full-matrix least-squares methods, on F^2's, in SHELXL [29]. The non-hydrogen atoms were

refined with anisotropic thermal parameters. All hydrogen atoms were located in difference maps and were refined isotropically and freely. Scattering factors for neutral atoms were taken from the literature [30]. Computer programs used in this analysis were noted above and run through WinGX [31]. Molecular diagrams were prepared using the ORTEP3 program [32]. Details on data collection, structure refinement and principal bond dimensions are presented in Tables S1 and S2.

2.3. Computational details

Quantum chemistry calculations were performed by DFT, using the ωB97XD functional [33] and the def2TZVP basis set [34] available in Gaussian16 [35]. The optimized geometries of the anion and triethylammonium cations of **I** were calculated separately, in both cases using the X-ray diffraction results as a basis. The molecular optimization was initially performed in vacuum, and the results were used as a starting point to the calculations in water through the conductor-like polarizable continuum model (CPCM) approach [36]. The calculated vibrational spectra have a good correlation with that recorded experimentally, corroborating the optimization of geometry. Atomic charges were calculated by the Bader scheme using the Multiwfn 3 program for wavefunction analysis [37]. The frontier orbitals were rendered by Chemcraft 1.8 [38]. The broken symmetry (BS) approach [39] was used in Gaussian16 to calculate the magnetic exchange coupling constant (*J*) involving the two metal ions in **I**.

2.4. Cell Culture

The human hepatocellular carcinoma (HepG2) cell line was acquired from the Rio de Janeiro Cell Bank, which is maintained by the Federal University of Rio de Janeiro and the Paul

Ehrlich Technical-Scientific Association in Brazil. The cells were grown in the high-glucose DMEM medium supplemented with 10% fetal bovine serum (FBS) and gentamycin (50 μg mL^{-1}). The medium was adjusted to pH 7.4 with sodium bicarbonate, and the culture was incubated at 37.0 ^{o}C in a humidified atmosphere containing 5% CO_2. After growing, the HepG2 cells were divided for use in the different treatment groups. Growth media containing 5.5 mM and 55 mM of glucose were employed to emulate the normal glycemia or the hyperglycemia conditions respectively; the hyperglycemic composition models insulin-resistance conditions in diabetic patients. All cell experiments were performed at 80 to 90% of cells confluence.

2.5. Cell Viability Assay

HepG2 cells were trypsinized, harvested and seeded (10^4 cells/well) in 96-well plates. After 24 h of adhesion, the culture medium was gently removed and a freshly-prepared solution of **I** (1000 μmol L^{-1}), diluted to the final concentrations of 600, 300, 100, 10, 1.0, and 0.10 μmol L^{-1} in DMEM, was added to the wells. The cells were incubated as described above for 24 and 48 h, and then washed once with phosphate-buffered saline (1 X PBS, pH 7.3) to remove the vanadium compound. Cell viability was determined with 3-(4,5-dimethylthiazol-2-yl)-2,5-diphenyltetrazolium bromide (MTT) [40] diluted with 1 X PBS to the final concentration of 0.5 mg mL^{-1} and added to each well. After 4 h of incubation at 37.0 °C, the formazan precipitate was dissolved in 100 μL of dimethylsulfoxide (dmso), and the absorbance of the resulting solution was measured at 570 nm. All assays were performed at least in triplicate. The IC_{50} values (concentration of **I** that promotes a 50% growth inhibition of HepG2 cells treated with **I** for 24 and 48 h) were calculated by fitting

curves to log values. Values reported in this work are the average of the responses obtained from three distinct experiments.

2.6. 2-NBDG Uptake Assay

The uptake of 2-NBDG, the fluorescent analog of D-glucose, by HepG2 cells was determined by adapting a previously described protocol [41, 42]. Briefly, cells were grown to 70–80% confluence, washed twice with phosphate-buffered saline (1 X PBS, pH 7.3), resuspended in DMEM in normal glucose (5.5 mmol L^{-1}) or hyperglycemic (55 mmol L^{-1}) conditions and then incubated in the absence or presence of **I** (0.10 and 0.50 µmol L^{-1}) for 24 h. Cells in normal glucose medium were used as the negative control, while those with the hyperglycemic medium containing 0.1 µmol L^{-1} of insulin were used as positive control. The optimal conditions for this assay were determined from a concentration curve (10 to 50 µmol L^{-1}), selecting the concentration giving the highest difference between the uptake in normal and hyperglycemic conditions [42]. The cultures were washed twice with 1 X PBS, and then incubated in glucose-free culture medium with the selected 2-NBDG (20 µmol L^{-1}) for 20 min. At the conclusion of the experiment, the 2-NBDG uptake was stopped by supernatant removal, after which the cells were washed twice, resuspended in cold 1 X PBS (300 µL), and analyzed by flow cytometry. For each measurement, data from 5000 single-cell events were collected using a FACSCalibur^{TM} platform with a 530/30 (FL1) filter. Differences between multiple groups were detected by one-way ANOVA corrected by Tukey [43]. The values were expressed as arithmetic averages, considering the standard deviation of three independent experiments. A value of $P < 0.05$ was considered statistically significant.

3. RESULTS AND DISCUSSION

3.1. Synthesis of product **I**

The synthesis of **I** was performed from V_2O_5 suspended in an aqueous solution of oxalic acid (60 °C, pH 1) to which 1,3-butanediol, a hypoglycemic agent, was subsequently added [44]. The final pH of the reaction mixture was adjusted to 7 by addition of triethylamine (Eq. 1), and greenish-blue crystals of **I** were isolated after workup. The product was only obtained in the presence of the diol, although the mechanistic role of this reagent in the system is still a matter of speculation. The powder X-ray diffraction pattern of the reaction product is in good correspondence with that predicted by using the single-crystal refined structure (Fig. S2), leading to the conclusion that the selected single crystal is representative of the whole batch of product **I**.

$$V_2O_5 + 4\,H_2C_2O_4 + 2\,Et_3N \rightarrow (Et_3NH)_2[\{VO(OH_2)(C_2O_4)\}_2(\mu\text{-}C_2O_4)] + 2\,CO_2 + H_2O$$

[Eq.1]

The standard potential, $E°$, of the VO_2^+/VO^{2+} pair is 1.00 V *vs.* SHE, which means that vanadium(V) can been reduced in acidic media by various organic and inorganic compounds such as hydroquinone, hypophosphorous acid, catechol, ascorbic acid, and oxalic acid, among others [45, 46]. This seems to be the case in the present system. Reduction of V_2O_5 by $H_2C_2O_4$ in acidic media, and in the absence of other redox-active species, produces the well-known mononuclear species VO(ox) and $VO(ox)_2^{2-}$ [45]. In close-to-neutral aqueous solutions, vanadium(IV) tends to suffer disproportionation, but this oxidation state may be stabilized by complexation. In the present work, the bidentate oxalate coordination mode, both in the

bridge and in the terminal ligand, together with a possible metal chelation by 1,3-bd in an early stage of the reaction, may have played a part in such stabilization. The actual role of 1,3-bd in the process is not yet well understood, given that it can participate in the redox process and that its intact form does not coordinate to the metal in the conditions used in this work.

3.2. Crystal structure

Complex **I** crystallizes in the monoclinic centrosymmetric space group $P2_1/n$. Its structure consists of an anionic binuclear complex formulated as $[\{VO(OH_2)(ox)\}_2(\mu\text{-}ox)]^{2-}$, with two triethylammonium counter ions (Fig. 1). A bis-bidentate oxalate ligand bridges the two six-coordinate vanadium centers, and the coordination sphere of each metal ion is completed by three terminal ligands: one bidentate oxalate, one water molecule and an oxide group.

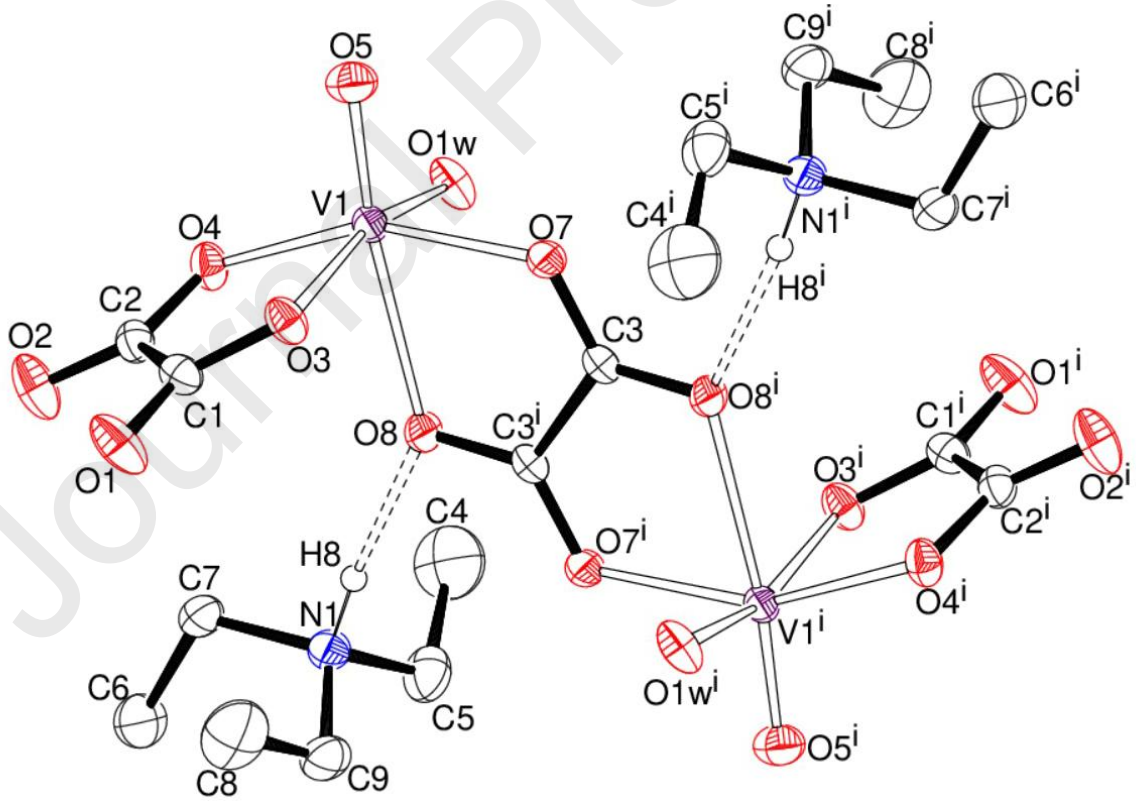

Figure 1. ORTEP-3 [32] representation of $(Et_3NH)_2[\{VO(OH_2)(ox)\}_2(\mu\text{-}ox)]$ (**I**), with the atom numbering scheme and thermal ellipsoids drawn at 50% probability. All hydrogen

atoms were omitted for clarity, except those involved in hydrogen bonds. Symmetry code: i : 1-x, 1-y, 1-z.

The literature contains four previous descriptions of the $[\{VO(OH_2)(ox)\}_2(\mu\text{-}ox)]^{2-}$ anion with similar structural data. The main differences are the presence or absence of crystallizing water molecules and in the nature of the counterions, viz. tetraethylammonium [46], tetraphenylphosphonium [47, 48], and the protonated form of 1,4-bis((3,5-dimethyl-1H-pyrazol-1-yl)methyl)benzene [49]. The intramolecular V···V distance through the bridging oxalate is 5.732 Å, significantly longer than the values ranging from 5.161 to 5.661 Å previously observed in similar dimers such as $[(VO)_2(\mu\text{-}ox)(OH_2)_6]^{2-}$ [50], $[(VO)_2(NCS)_6(\mu\text{-}ox)]^{4-}$ [50], $[\{VO)_2(OH)(OH_2)\}_2(\mu\text{-}ox)]$ [51] and the complex $[(CpP^{OMe}Co)VO]_2(\mu\text{-}ox)]$ [52] containing $(CpP^{OMe}Co)^-$ as a ligand.

The Et_3NH^+ cations and coordinated water molecules interact with the bridging oxalate ligands of **I** through strong hydrogen bonds [N(1)–H(8)···O(8), O(1w)–H(19)···O(1') and O(1w)–H(21)···O(2'')], with H···O distances that range from 1.84 to 1.98 Å and angles from 168 to 174 ° (Fig. S3 and Table S3). Three weak C–H···O bonds involving the cation and the coordinated oxygen atoms on the terminal oxalate ions were also identified. Additional comments on the structure of **I** are presented as Supplementary Material, along with complementary crystallographic and structural data in Tables S1 and S2.

3.3. Geometry optimization

The ωB97XD functional and the def2TZVP basis set were chosen for DFT calculations because of their well-known ability to reproduce the structural and spectroscopic data

obtained experimentally for transition metal complexes [53]. The bond lengths and angles from the optimized geometry are close to those measured in the solid-state (see selected data in Tables 1 and S4). Also, considering that the geometry optimized in water (with the CPCM model) was closer to the crystallographic results than that calculated in vacuum, it was selected to provide information about the electronic structure, Bader charges on atomic centers, and theoretical vibrational and electronic spectra of **I**.

Table 1. Comparison between selected bond lengths (Å) and angles (°) obtained for **I** by single crystal X-ray diffraction analysis (XRD) and optimized by DFT calculations of the $[\{VO(OH_2)(ox)\}_2(\mu\text{-}ox)]^{2-}$ anion in water

Bond lengths / (Å)					
	XRD	**DFT**		**XRD**	**DFT**
V(1)–O(5)	1.5859(13)	1.5745	V(1)–O(4)	1.9734(12)	1.96301
V(1)–O(3)	1.9882(12)	1.9595	V(1)–O(1w)	2.0252(14)	2.1405
V(1)–O(7)	2.0477(12)	2.0552	V(1)–O(8)#1	2.3488(12)	2.3011
Angles / (°)					
	XRD	**DFT**		**XRD**	**DFT**
O(1w)–V(1)–O(7)	89.71(6)	91.4	O(4)–V(1)–O(1w)	90.48(6)	89.8
O(1w)–V(1)–O(8)	81.25(6)	73.9	O(5)–V(1)–O(7)	98.42(6)	97.8
O(3)–V(1)–O(7)	90.79(5)	89.3	O(5)–V(1)–O(1w)	98.55(7)	93.1
O(4)–V(1)–O(3)	81.52(5)	81.7	O(3)–V(1)–O(1w)	161.12(6)	159.9
O(5)–V(1)–O(4)	105.20(6)	105.5	O(4)–V(1)–O(7)	156.07(5)	156.5
O(7)–V(1)–O(8)	74.09(4)	74.7			

Consistently with the experimental X-ray structure, the oxidovanadium(2+) groups and the bis-bidentate oxalate bridge in the DFT-optimized structure of **I** lie in the molecular (equatorial) plane, while the terminal oxalate and the water ligands are positioned perpendicular to this plane (Fig. 2).

3.4. Charges and spin density on atomic centers

The Atoms In Molecules (AIM) charge model [54], also known as Bader´s charges, provides a realistic understanding of how electrons are partitioned between bound atoms in a molecule [55]. In **I**, because of the centrosymmetric nature of the complex anion, charges on equivalent atoms are not shown in Fig. 2a. For the vanadium atoms, charge donation from the ligands to the polarizing metal center agrees with the lowering of the formal value of 4+. Consistent with this observation, the negative charges on the vanadyl oxygens (−1.021 O(5) a.u.) are less negative than 2−. The calculated charge values for all oxalate oxygen atoms, in turn, are lower but close to 2−, an observation that can be attributed to the relocation of electron density from the neighboring vanadium and carbon centers. The relocation from carbon is more relevant for the oxygen donor atoms of the bridging ligand.

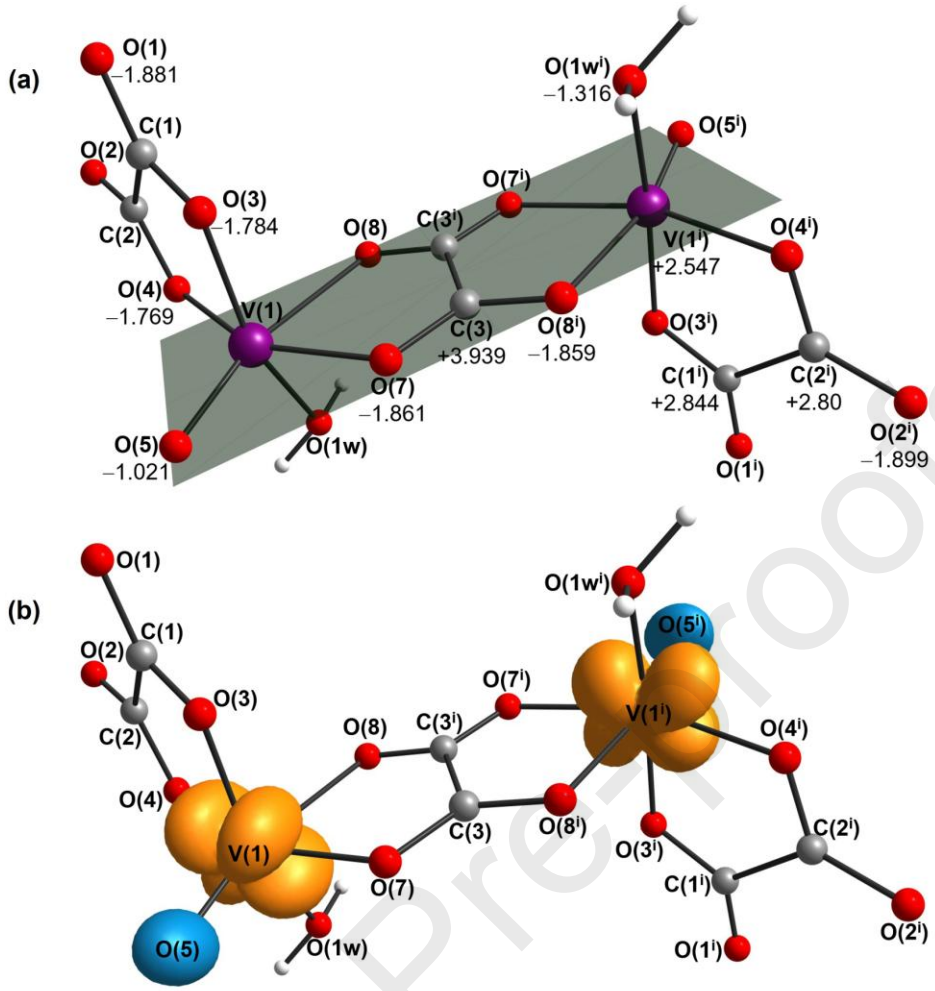

Figure 2. The optimized geometry of the binuclear anion in **I**, showing (a) the Bader charges, and (b) the spin density difference map (orange and blue colors represent positive and negative values, respectively).

Figure 2b shows partial spin density delocalization from the vanadium centers to the oxo groups (Fig. 3b), in line with the paramagnetic nature of the d^1 metal ions and their strong sigma and pi interactions with the ligand.

The binuclear structure of complex **I**, built by interaction of the two V^{IV} ions (S = ½) through the oxalate bridge, prompted an investigation of a potential magnetic exchange coupling involving the metal ions. Literature reports (Table S5) describe the existence of such an exchange in other centrosymmetric dimers containing the $\{VO(\mu\text{-ox})VO\}^{2+}$ core, investigated by magnetic susceptibility measurements in the solid state and/or theoretical calculations [46,

47, 50, 56]. The data in Table S5 refer to complexes in which, similarly to **I** (Fig. 2), the two V=O groups occupy *trans* positions (relative to one another) in the equatorial plane that contains the bridging ligand. In all cases listed in the table, the magnetic exchange coupling constant (*J*) is small and compatible with weak antiferromagnetic coupling. Other relative arrangements of the VO^{2+} groups in oxalate-bridged dimers, and their magnetic interaction, have been the subject of theoretical studies [15].

In the case of complex **I,** an exchange coupling constant (*J*) value of –3,61 cm^{-1}, calculated by the broken symmetry approach with the same functional and basis set employed for geometry optimization (ωB97XD/def2TZVP), also support the presence of weak antiferromagnetic exchange propagated between the two S = ½ spins. This result agrees with the experimental $\chi_M T$ value of 0.698 emu K mol^{-1} determined for powdered **I** at 297 K (χ_M stands for the molar magnetic susceptibility and T the absolute temperature). This value is lower than the expected (0.75 emu K mol^{-1}) for two independent, non-coupled d^1 ions considering g = 2.00 [57]. This finding is also compatible with the nature of the magnetic orbitals involving the two V^{IV} centers (see the frontier orbitals in Fig. 3), which overlap the bridging oxygen orbitals only in the π mode, resulting in weak magnetic coupling [46]. In Table S5, although the largest non-bonding V···V distance in **I** appears to correlate with the least negative *J* value, and therefore the weakest coupling, the lack of more abundant data on similar, structurally characterized complexes prevents further analysis.

3.5. Frontier orbitals and electronic spectra

Fig. 3 presents the calculated contour surfaces for selected frontier orbitals ranging from the singly-occupied molecular orbital SOMO–2 and the associated unoccupied SUMO+2. It can

be noted that the vanadium centers and terminal oxalate ligands contribute significantly to the SOMO and SOMO−1, while the bridging oxalate participates in the composition of the SOMO−2. The significant contribution of the oxidovanadium(2+) groups (V=O) to the unoccupied frontier orbitals is noteworthy, and such contribution cannot be seen in the occupied ones. The SUMO lacks the contribution of the terminal ox^{2-} ligands, being, in turn, distinguished by the participation of the bridging oxalate, particularly of the σ C–C bond. Contour surfaces for other frontier orbitals are presented in Table S6.

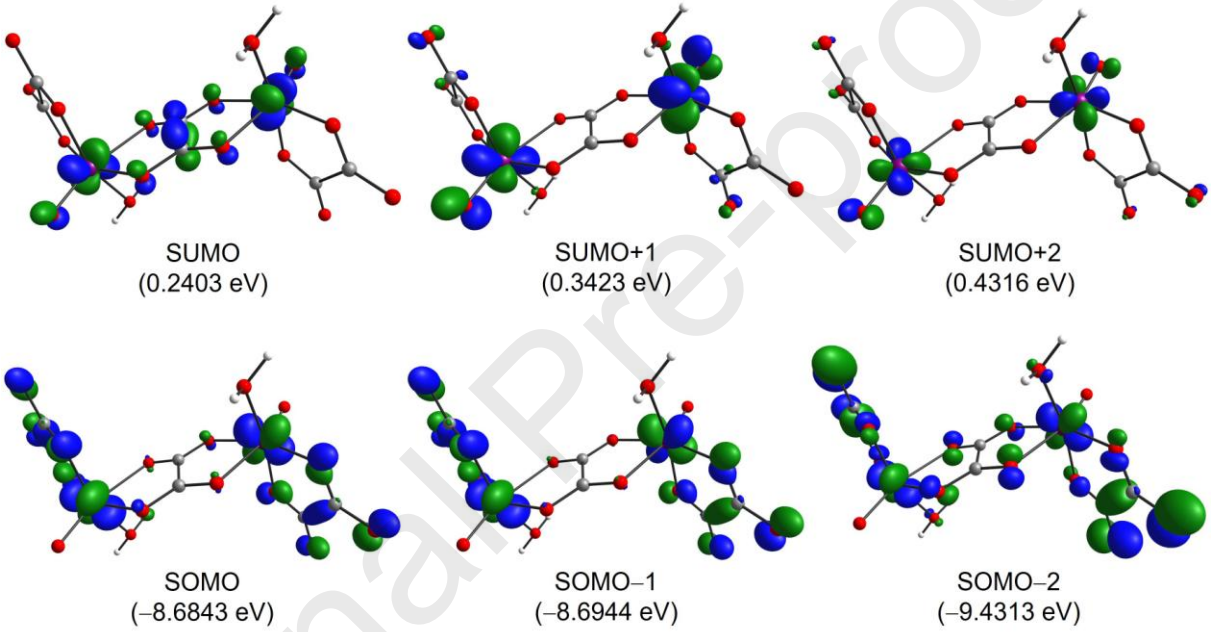

Figure 3. Graphic representation of selected frontier molecular orbitals of **I**. Colors: red = oxygen, purple = vanadium, gray = carbon and white = hydrogen.

The electronic spectrum of **I** (Fig. S4) presents an intense band below 460 nm and two d-d bands with maximum absorbances at 620 and 785 nm, which are characteristic of oxidovanadium(2+) complexes in distorted octahedral geometry [58]. The calculated electronic spectrum, in turn, presents three d-d bands at 753, 638 and 502 nm, attributed mainly to $d_{xy} \rightarrow (d_{xz}, d_{yz})$, $d_{xy} \rightarrow d_{x^2-y^2}$ and $d_{xy} \rightarrow d_{z^2}$ transitions. The wavelengths, energies and oscillator strengths obtained for the calculated transitions are presented in Table 2. The

two d-d bands calculated at the lowest energies are observed in the experimental spectrum, while the third one is masked by the intense band registered below 450 nm (calculated at 322 nm) and assigned to a ligand-to-metal charge transfer (LMCT) transition [58].

Table 2. Wavelengths, energies, oscillator strengths, orbital contributions and assignments of frontier orbital transitions calculated for **I** by DFT with the ωB97XD functional and the def2TZVP basis set. Excitations are listed if their contribution to the state is higher than 10%

Wavelength (nm)	Energy (eV)	Oscillator strength (*f*)	Frontier orbital transition	Contribution (%)	Assignment of orbital distribution
753	1.6459	0.0010	SOMO → SUMO SOMO–1 → SUMO+1	24 20	d–d transition
638	1.9418	0.0011	SOMO → SUMO+2 SOMO–1 → SUMO+3	27 20	d–d transition
502	2.4644	0.0003	SOMO → SUMO+8 SOMO–1 → SUMO+7	32 27	d–d transition
322	3.8405	0.0257	SOMO–1 → SUMO+4 SOMO–2 → SUMO+4	19 18	LMCT transition

3.6. Vibrational Spectroscopy

The experimental and calculated FTIR and Raman spectra of complex **I** are presented in Fig. 4, and the tentative band assignments are listed in Table 3. The FTIR spectrum registered for **I** shows bands from 989 to 480 cm^{-1} attributed to ν(V=O), ν_{as}(V–O), ν_{s}(V–O) and δ_{as}(V–O) [59-61]. Bands for ν(CO), ν(CC) and δ(OCO) can be observed from 1691 to 1147 cm^{-1}. The calculated spectrum of the triethylammonium cation complements the spectrum of the binuclear anion, resulting in a substantial similarity with the experimental data. The broad bands located around 3415 cm^{-1} are assigned to ν(N–H) from the triethylammonium cations and ν(O–H) from the coordinated water. The Raman spectrum shows bands related to ν(N–H)

from the triethylammonium cations at 2947 and 2984 cm^{-1}. Bands between 1681 and 1081 cm^{-1} originate from oxalate vibrations [62-64], and those located between 995 and 280 cm^{-1} are attributed to ν(V=O), ν_{as}(V-O), ν_{s}(V-O) and δ_{as}(V–O). The largest differences between the experimental FTIR and Raman spectra and the calculated bands occur for the O–H and N–H modes close to 4000 cm^{-1} (see Table 3), because the calculations were carried out at the single molecule level, excluding intermolecular interactions such as hydrogen bonds. Band assignments shown in Table 3 were based on the calculated spectra and on literature data [59-64].

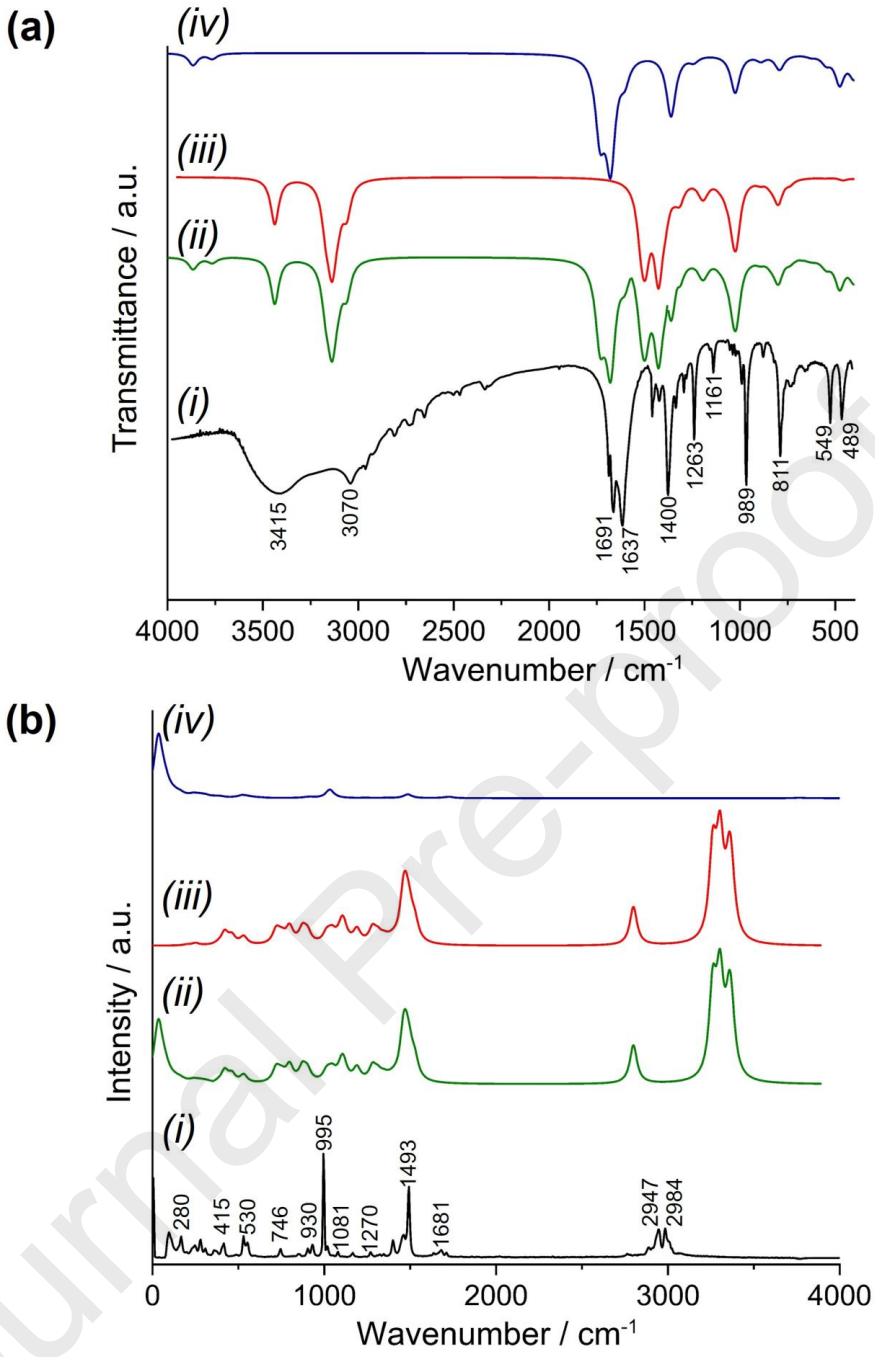

Figure 4. ***(a)*** FTIR and ***(b)*** Raman spectra: *(i)* recorded for **I** (black line); *(ii)* calculated for the complex by adding the spectra of cation and anion (green line); *(iii)* calculated only for the triethylammonium cation (red line); and *(iv)* calculated for the binuclear anion in **I** (blue line).

Table 3. Tentative assignments for the FTIR [59-61] and Raman [62-64] vibrational modes in the spectra registered for **I**, based on the literature and DFT calculations

FTIR			Raman		
Tentative assignment	**Experimental / cm^{-1}**	**Calculated / cm^{-1}**	**Tentative assignment**	**Experimental / cm^{-1}**	**Calculated / cm^{-1}**
ν(O–H)	3415	3919	ν(N–H)	2984 and 2947	3473
ν(N–H)	3415	3473	ν(C=O)	1681	1711
ν(C–O)	1637 and 1691	1711	ν(CO) + ν(CC)	1493	1530
ν(CO)	1400	1404	ν(CO) + δ(O–C=O)	1399	1404
$\nu(CO_2)$	1263	1273	ν(C–N)	1270	1316
ν(C–H)	1161	1192	ν(C–H)	1166	1113
ν(V=O)	989 and 1010	1077 and 1085	ν(C–C)	1081	1084 and 1092
ν(V–O)	811	811 and 816	ν(V=O)	995	1077 and 1085
ν(V–O) and δ(V–O)	549 and 489	530 and 562	ν_{as}(V–O)	930	941
			ν_{s}(V–O)	530	530
			δ(V–O)	415 and 280	412 and 290

ν = symmetric and asymmetric stretching; δ = symmetric and asymmetric angular deformation.

3.7. Electronic Paramagnetic Resonance (EPR) in solid-state and solution

The X-band EPR spectrum registered for a pulverized sample of **I** (Fig. S6) at 77 K exhibits a broad line at 338 mT (g = 1.987 and Δ_{pp} = 7.2 mT) with no observable hyperfine pattern. This profile is compatible with the binuclear nature of product **I**, which contains vanadium(IV) ions ($3d^1$, I = 7/2), in the solid state, and confirms the reduction of the vanadium(V) derived from V_2O_5 [65]. The aqueous solution spectra, in turn, were recorded at 77 K in both freshly-prepared samples (Fig. 5a) and after 24 h of exposition to the air (Fig. S7), in concentrations ranging from 0.1 to 2.0 mmol L^{-1}. In all concentrations and times, a broad line with g = 1.986 and Δ_{pp} = 23.1 mT was observed, in agreement with the expected ΔMs = ± 1 transition of a binuclear species. This result suggests the maintenance of the binuclear structure in pure aqueous solutions of **I** over the time period of the experiment [65].

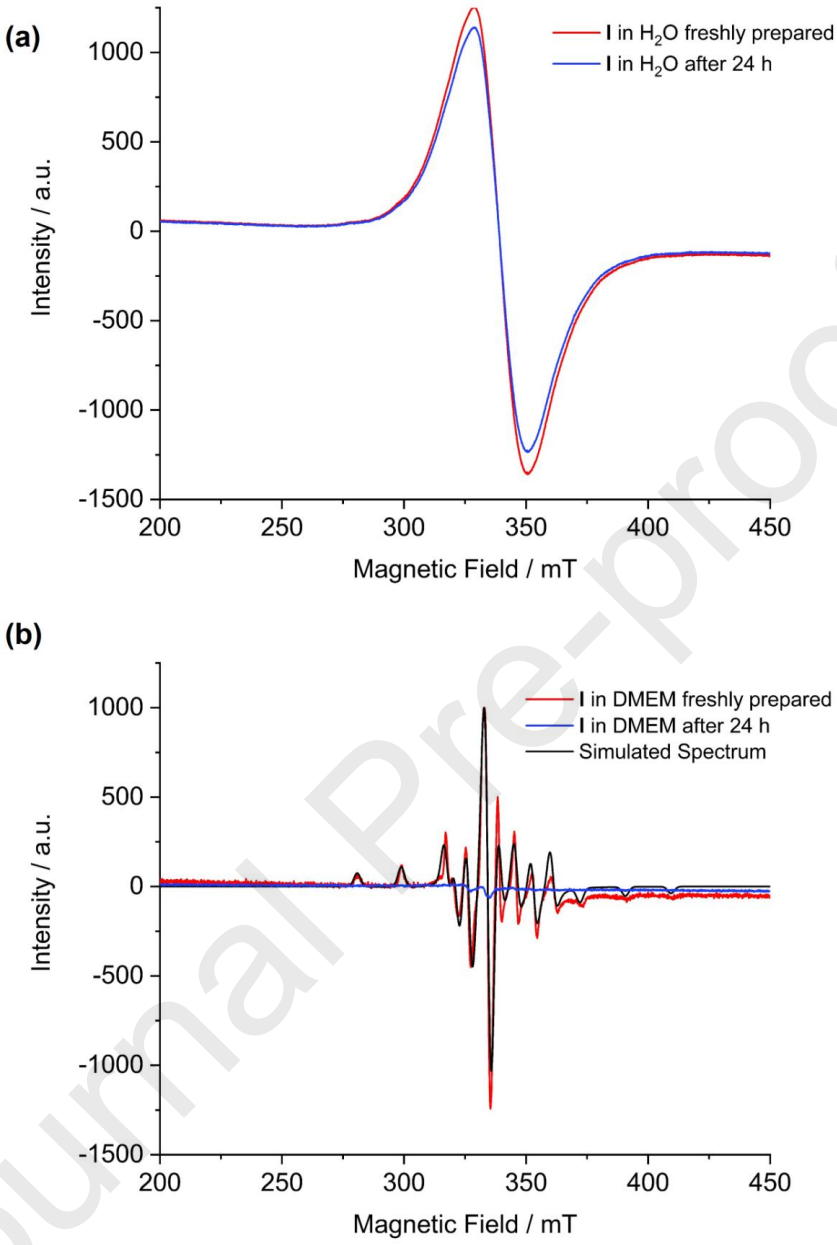

Figure 5. X-band EPR spectra registered at 77K for **I** (a) from 2.0 mmol L^{-1} aqueous solutions in a freshly prepared sample (red line) and after 24 h (blue line) of exposition to the air; (b) from a 2.0 mmol L^{-1} solution freshly prepared in DMEM (red line) and after 24 h (blue line). The black line in (b) corresponds to the simulated spectrum.

On the other hand, the spectrum of **I** registered at 77 K in the culture medium DMEM showed an anisotropic hyperfine pattern that is typical of a mononuclear vanadium(IV) species in frozen solution (Fig. 5b), evidencing the breakage of the binuclear structure. The values of the EPR parameters $g_{\perp} = 1.946$, $g_{\parallel} = 1.975$, $A_{\perp} = 50.2 \times 10^{-4}$ cm^{-1}, and $A_{\parallel} = 169.3 \times 10^{-4}$ cm^{-1} are different from those reported for the aqueous vanadyl cation $[VO(OH_2)_5]^{2+}$ ($g_{\perp} = 1.936$, $g_{\parallel} = 1.976$, $A_{\perp} = 66.4 \times 10^{-4}$ cm^{-1}, and $A_{\parallel} = 177.2 \times 10^{-4}$ cm^{-1}) [66]. It is probable that the vanadium(IV) species detected in DMEM is formed by reaction of **I** with one of the coordinating components of the culture medium, generating a mononuclear vanadium(IV) species such as $[VOL'_x]^{n+/n-}$. It is worth emphasizing that DMEM has a complex composition, containing various vitamins, aminoacids and other potential *N*- and *O*-donor ligands [67].

In the literature, the reactivity of vanadium compounds such as the orthovanadate anion and bis(methylmaltolato)oxidovanadium(IV), BMOV, with components of DMEM was studied by X-ray absorption near-edge structure spectroscopy (XANES). Results showed that small variations in the composition of the medium led to dramatic changes in the vanadium coordination environment [68]. These differences gradually disappeared with time due to oxidation of the metal ions, and, after 24 h, both prodrugs rendered products containing *ca.* 75% of V^{V} and 25% of V^{IV}. In the present work, complex **I** dissolved in DMEM presents an even more extensive oxidation of V^{IV} to V^{V} after 24 h, as evidenced by the significant decrease in the intensity of its EPR spectrum (Fig 5b, blue line). This result confirms that complex **I** is more resistant to structural changes and oxidation in pure water than in the rich DMEM culture medium; future mechanistic studies of biological activity should take these data into account.

3.8. Evaluation of the anti-diabetic effect of **I** in HepG2 cells

The goal of these experiments was to assess whether solutions of **I** in DMEM stimulate glucose uptake by HepG2 cells *in vitro*, using 2-NBDG as a fluorescent indicator for direct uptake measurement. The assays were performed in three steps: *(i)* evaluation of the *in vitro* cytotoxicity of **I** on HepG2 cells; *(ii)* determination of the best concentration of 2-NBDG to be employed *in vitro*, based on known levels of D-glucose in healthy and diabetic individuals; *(iii)* evaluation of the influence of **I** on 2-NBDG uptake using flow cytometry and detecting the resulting fluorescence produced by the cells [42].

The effect of **I** on the HepG2 cell viability was evaluated after 24 and 48 h of incubation, and compared with the control with non-treated HepG2 cells. The IC_{50} value of 15.67 μmol L^{-1}, determined for **I** after 24 h to help designing the subsequent experiments (Fig. S8), is in the range reported for other vanadium(IV) complexes in similar conditions (from 7.35 to 47.21 μmol L^{-1}) [18, 69, 70] (Table S7). Based on these results, the potential anti-diabetic effect of **I** was evaluated in concentrations lower them the IC_{50}. We observed that **I** was non-toxic up to 1.0 μmol L^{-1} over the time course of the cell studies, and its cytotoxicity decreased after 48 h, probably due to precipitation of a vanadium-containing species from the culture media. In fact, a blue solid, supposedly containing vanadium, was observed in the culture at the end of the experiment, possibly decreasing the vanadium availability to the cells. This blue solid has not been isolated and characterized so far, due to its reduced amount.

From the data described above, it was possible to select the conditions to be applied in the subsequent assays, viz. 24 h of incubation and concentrations of 0.50 and 0.10 μmol L^{-1} for **I**,

which correspond to 50% and 10% of the toxicity threshold (1.0 μmol L^{-1}). The (control) uptake assays of 2-NBDG by the HepG2 cells were carried out by fixing two concentrations of D-glucose in the culture media: (i) 5.5 mmol L^{-1}, aiming to simulate the conditions found in cells of healthy individuals, and 55 mmol L^{-1} for the hyperglycemic model. The measurement of 2-NBDG uptake was performed with 10, 20, 30 and 50 μmol L^{-1} of the fluorescent tracer (Fig. S9). The highest difference in uptake between the two culture conditions was obtained with 20 μmol L^{-1} of 2-NBDG; this concentration was used in the assays to determine the effect of insulin and the vanadium compound.

The uptake of 100% of 2-NBDG reflects control cells (first column in Fig. 6) with normal performance for glucose internalization. In contrast, in the hyperglycemic medium, the uptake decreased by 41% (first two columns in Fig. 6), establishing a condition similar to insulin-resistance in diabetic individuals. The addition of insulin (0.10 μmol L^{-1}) to the hyperglycemic medium enhanced the uptake of 2-NBDG by cells, reflected in a 27% increase compared to the hyperglycemic medium alone. Finally, similar 2-NBDG uptake assays were performed in hyperglycemic conditions using the two selected concentrations of **I** (0.5 and 0.1 μmol L^{-1}, Fig. 6). Compound **I** showed a positive effect on 2-NBDG uptake that is similar to that of insulin, reaching average uptake percentages up to 91 % (blue bars) ($P < 0.001$).

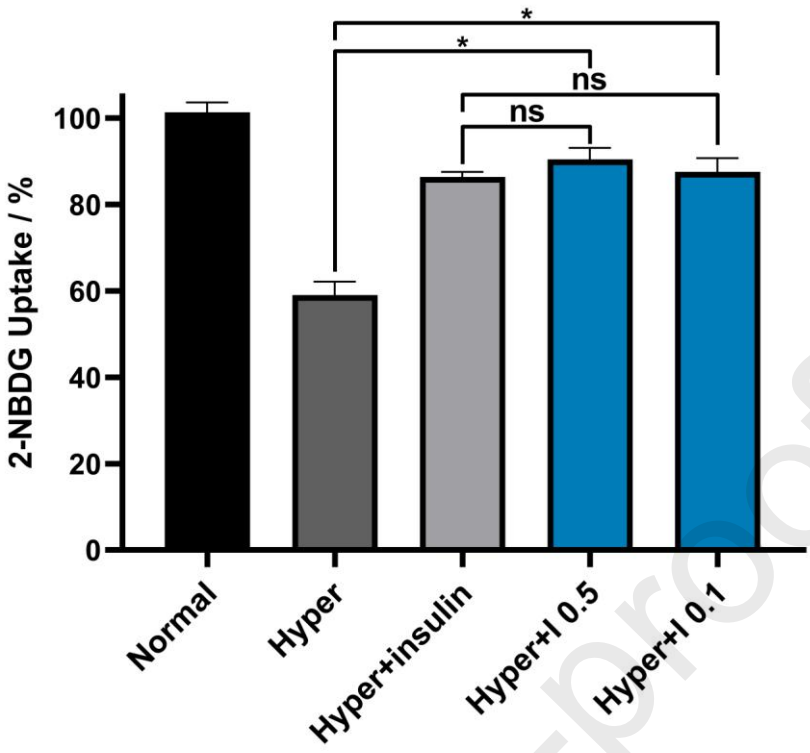

Figure 6. Uptake of 2-NBDG by HepG2 cells under different culture conditions. All cells were first cultivated in DMEM, in the presence or absence of **I**, for 24 h at 37 °C. The glucose analog 2-NBDG (20 μmol L^{-1}) was added 20 min before the cytometry analysis. The vertical bars are mean ± SD of the fluorescence percentage of the HepG2 cells compared to the control (100%). The first three bars are control assays that correspond to normal uptake conditions (glucose, 5.5 mmol L^{-1}) in black; hyperglycemic medium (glucose, 55 mmol L^{-1}) in gray; and hyperglycemic medium with 0.10 μmol L^{-1} of insulin, in light gray. The blue bars represent assays in hyperglycemic media with added 0.10 and 0.50 μmol L^{-1} of **I**. These data were obtained from three independent experiments. P-values, ANOVA corrected by Tukey, *P<0.001 and ns = non–significant.

The insulin-mimetic or insulin-enhancer effect of vanadium compounds has been demonstrated *in vitro* for different cell models and culture conditions [3, 6]. The vast majority of these compounds are neutral bis-chelate complexes of vanadium(IV) with (O,O)-, (O,N)-, (O,S)- or (N,N)-donor ligands, which suffer fast ligand exchange reactions in aqueous medium [6]. It is well established that such vanadium compounds have an influence on the insulin-signaling pathways [3, 5], inducing or enhancing the phosphorylation of proteins or enzymes such as kinase B (PKB), glycogen synthase kinase-3 (GSK-3), and forkhead box

protein 1 (FoxO1) [71]. Despite these findings, only a few studies [72, 73] assessed the effect of vanadium compounds in the uptake of 2-NBDG by cells, and the variations in cell lines and in the standard anti-diabetic drug used as references in the existing protocols render comparisons difficult or ambiguous. Among the literature reports, two studies summarized in Table 4 demonstrated the potential of vanadium complexes to enhance (up to 95%) the uptake of 2-NBDG by cell cultures [72, 73]. The low concentrations of vanadium necessary to improve the 2-NBDG uptake deserve attention, particularly in the case of **I** in which the enhancement activity is observed in non-toxic concentrations.

Table 4. *In vitro* studies of insulin-mimetic action quantified by 2-NBDG uptake after 24 h of incubation in the presence of vanadium complexes

Vanadium compound (μmol L^{-1})	**Cell line**	**Standard anti-diabetic drug (μmol L^{-1})**	**2-NBDG (μmol L^{-1})**	**% of uptake**	**Ref**
$[VO(hpdbal\text{-}an)_2]$ 0.20	HepG2	Metformin 0.20	100	95	[72]
$[VO(otp)_2]$ 0.10	3T3–L1	Insulin 0.10	40	95	[73]
$(Et_3NH)_2[\{VO(OH_2)(ox)\}_2(\mu\text{-}ox)]$ (**I**) 0.10 and 0.50	HepG2	Insulin 0.10	20	91	#

hpdbal = 2,2'-((ethane-1,2-diylbis(azanediyl))bis(methylene))bis(4-(phenyldiazenyl)phenol)), and otp = pyridoxylidenetryptamine. # This Work.

It was recently demonstrated that $VOSO_4$ promotes the generation of the $^{\bullet}OH$ radical in HepG2 cells, increasing intracellular levels of reactive oxygen species (ROS) in a dose-dependent manner; this is essential for triggering the signaling response of insulin [8]. In the context of the present work, the promising results obtained for **I** open the way for the investigation of the active vanadium species formed in DMEM (and observed by X-band EPR), both in terms of chemical nature and general occurrence, particularly when starting from other water-soluble vanadium(IV) complexes.

4. CONCLUSION

This work described the synthesis, in good yield, and characterization, by single-crystal XRD and spectroscopic methods, of a highly water-soluble, binuclear oxalate-bridged oxidovanadium(IV) complex (**I**). The product was obtained by reaction of V_2O_5 with oxalic acid in the presence of 1,3-butanediol, which led to the reduction of vanadium(V) and the incorporation of oxalate anions both as terminal and bridging ligands. The binuclear structure of **I** was maintained in aqueous solution, even in low concentrations. In the DMEM culture medium, in turn, **I** apparently gives rise to a mononuclear vanadium(IV) complex that could be the active species responsible for the potential anti-diabetic activity reported in this work.

Glucose uptake by cells plays a fundamental role in diabetes mellitus research. Our results showed a significant increase (*ca.* 32%) in the uptake of 2-NBDG by HepG2 cells treated with **I** in comparison to the uptake observed in non-treated culture cells. This effect is comparable to that caused by insulin in hyperglycemic media. Further experiments are needed to investigate the chemical nature of the active species under physiological conditions and the mechanism of action at the molecular level, looking for targets in the insulin signaling pathway and assessing the anti-diabetic potential of **I** *in vivo*.

CONFLICTS OF INTEREST

There are no conflicts to declare.

APPENDIX A

Supplementary data

CCDC 2021322 contains the supplementary crystallographic data for complex **I**. These data can be obtained free of charge via http://www.ccdc.cam.ac.uk/conts/retrieving.html, or from the Cambridge Crystallographic Data Centre, 12 Union Road, Cambridge CB2 1EZ, UK; fax: (+44) 1223-336-033, or e-mail: deposit@ccdc.cam.ac.uk.

ACKNOWLEDGMENTS

Authors thank Mr. Ângelo Roberto dos Santos Oliveira (UFPR) for the TGA analyses, Ms. Rubia C. R. Bottini, from LAMAQ/UTFPR, for the metal analyses, and Ms. Kahoana Postal, Juliana M. Missina and Luana C. Camargo (UFPR) for helping with the EPR spectroscopy measurements. This project was supported by the Brazilian CNPq - Conselho Nacional de Desenvolvimento Científico e Tecnológico (Grant 308426/2016-9) and Fundação Araucária. Fellowships were financed by CAPES (Finance Code 01).

REFERENCES

[1] D. Rehder, The potentiality of vanadium in medicinal applications, Inorg. Chim. Acta, 504 (2020) 119445.
[2] A. Scibior, L. Pietrzyk, Z. Plewa, A. Skiba, Vanadium: Risks and possible benefits in the light of a comprehensive overview of its pharmacotoxicological mechanisms and multi-applications with a summary of further research trends, J. Trace Elem. Med. Biol., (2020) 126508.
[3] S. Treviño, A. Diaz, Vanadium and insulin: Partners in metabolic regulation, J. Inorg. Biochem., (2020) 111094.
[4] K.H. Thompson, J. Lichter, C. LeBel, M.C. Scaife, J.H. McNeill, C. Orvig, Vanadium treatment of type 2 diabetes: A view to the future, J. Inorg. Biochem., 103 (2009) 554-558.
[5] X. Wang, T. Sun, J. Liu, Z. Shan, Y. Jin, S. Chen, W. Bao, F.B. Hu, L. Liu, Inverse association of plasma vanadium levels with newly diagnosed type 2 diabetes in a chinese population, Am. J. Epidemiol., 180 (2014) 378-384.
[6] T. Jakusch, T. Kiss, In vitro study of the antidiabetic behavior of vanadium compounds, Coord. Chem. Rev., 351 (2017) 118-126.
[7] M. Xie, D. Chen, F. Zhang, G.R. Willsky, D.C. Crans, W. Ding, Effects of vanadium(III, IV, V)-chlorodipicolinate on glycolysis and antioxidant status in the liver of STZ-induced diabetic rats, J. Inorg. Biochem., 136 (2014) 47-56.

[8] Q. Zhao, D. Chen, P. Liu, T. Wei, F. Zhang, W. Ding, Oxidovanadium(IV) sulfate-induced glucose uptake in HepG2 cells through IR/Akt pathway and hydroxyl radicals, J. Inorg. Biochem., 149 (2015) 39-44.
[9] G.-H. Qiu, X. Xie, F. Xu, X. Shi, Y. Wang, L. Deng, Distinctive pharmacological differences between liver cancer cell lines HepG2 and Hep3B, Cytotechnology, 67 (2015) 1-12.
[10] W.-M. Yang, K.-H. Min, W. Lee, MiR-1271 upregulated by saturated fatty acid palmitate provokes impaired insulin signaling by repressing INSR and IRS-1 expression in HepG2 cells, Biochem. Biophys. Res. Commun., 478 (2016) 1786-1791.
[11] S. Knasmüller, V. Mersch-Sundermann, S. Kevekordes, F. Darroudi, W. Huber, C. Hoelzl, J. Bichler, B. Majer, Use of human-derived liver cell lines for the detection of environmental and dietary genotoxicants; current state of knowledge, Toxicology, 198 (2004) 315-328.
[12] D. Rehder, Vanadium in health issues, ChemTexts, 4 (2018) 20.
[13] S.-S. Zhu, X. Dong, Z.-H. Zhou, Mixed ligand oxidovanadium(IV) complexes: Synthesis, spectral, structural characterization and catalytic degradations of methyl orange, Inorg. Chim. Acta, 486 (2019) 395-400.
[14] A. Pokutsa, Y. Kubaj, A. Zaborovskyi, D. Maksym, T. Paczesniak, B. Mysliwiec, E. Bidzinska, J. Muzart, A. Sobkowiak, V^{IV}-catalyzed cyclohexane oxygenation promoted by oxalic acid: Mechanistic study, Mol. Catal., 434 (2017) 194-205.
[15] M. Perić, M. Zlatar, M. Gruden-Pavlović, S. Grubišić, Density functional theory study of the magnetic coupling interaction in a series of binuclear oxalate complexes, Monatsh. Chem. Chem. Mon., 143 (2012) 569-577.
[16] H. Sehimi, B. Essghaier, E. Barea, N. Sadfi-Zouaoui, M.F. Zid, Synthesis, structural study, magnetic susceptibility and antimicrobial activity of the first (μ-oxo)-bis(oxalato)-vanadium(IV) 1D coordination polymer, J. Mol. Struct., 1175 (2019) 865-873.
[17] I.E. León, S.B. Etcheverry, B.S. Parajón-Costa, E.J. Baran, Bis(oxalato)dioxovanadate(V) and bis(oxalato)oxoperoxo-vanadate(V) complexes: Spectroscopic caracterization and biological activity, Biol. Trac. Elem. Res., 155 (2013) 295-300.
[18] L. Ni, H. Zhao, L. Tao, X. Li, Z. Zhou, Y. Sun, C. Chen, D. Wei, Y. Liu, G. Diao, Synthesis, *in vitro* cytotoxicity, and structure–activity relationships (SAR) of multidentate oxidovanadium(IV) complexes as anticancer agents, Dalton Trans., 47 (2018) 10035-10045.
[19] W. Maret, A. Wedd, Binding, transport and storage of metal ions in biological cells, Royal Society of Chemistry, first ed., Cambridge, 2014.
[20] D. Stinghen, M. Atzori, C.M. Fernandes, R.R. Ribeiro, E.L. De Sá, D.F. Back, S.O. Giese, D.L. Hughes, G.G. Nunes, E. Morra, A rare example of four-coordinate nonoxido vanadium(IV) alkoxide in the solid state: Structure, spectroscopy, and magnetization dynamics, Inorg. Chem., 57 (2018) 11393-11403.
[21] J.M. Missina, B. Gavinho, K. Postal, F.S. Santana, G. Valdameri, E.M. De Souza, D.L. Hughes, M.I. Ramirez, J.F. Soares, G.G. Nunes, Effects of decavanadate salts with organic and inorganic cations on escherichia coli, giardia intestinalis, and vero cells, Inorg. Chem., 57 (2018) 11930-11941.
[22] J.M. Missina, L.B. Leme, K. Postal, F.S. Santana, D.L. Hughes, E.L. De Sá, R.R. Ribeiro, G.G. Nunes, Accessing decavanadate chemistry with tris(hydroxymethyl)aminomethane, and evaluation of methylene blue bleaching, Polyhedron, 180 (2020) 114414.
[23] D. Althumairya, K. Postal, G. Barisas, G.G. Nunes, D.A. Roess, D.C. Crans, Polyoxometalates function as indirect activators of a G protein-coupled receptor, Metallomics, (2020).

[24] C.F. Macrae, I. Sovago, S.J. Cottrell, P.T. Galek, P. McCabe, E. Pidcock, M. Platings, G.P. Shields, J.S. Stevens, M. Towler, Mercury 4.0: From visualization to analysis, design and prediction, J. Appl. Crystallogr., 53 (2020) 226-235.
[25] D. Evans, A new type of magnetic balance, J. Phys. E: Sc. Instrum., 7 (1974) 247.
[26] G.A. Bain, J.F. Berry, Diamagnetic corrections and Pascal's constants, J. Chem. Educ., 85 (2008) 532.
[27] A. Bruker., APEX3 Package, APEX3, SAINT and SADABS, (2016).
[28] G.M. Sheldrick, SHELXT–Integrated space-group and crystal-structure determination, Acta Crystallogr., Sect. A: Found. Adv., 71 (2015) 3-8.
[29] G.M. Sheldrick, Crystal structure refinement with SHELXL, Acta Crystallogr., Sect. C: Struct. Chem., 71 (2015) 3-8.
[30] D.C. Creagh, W. Mcauley. International tables for crystallography. AJC Wilson, Kluwer Academic Publishers, Boston, 4, 200-206, 1992.
[31] L.J. Farrugia, WinGX and ORTEP for Windows: an update, J. Appl. Crystallogr., 45 (2012) 849-854.
[32] M.N. Burnett, C.K. Johnson, ORTEP-III: Oak Ridge thermal ellipsoid plot program for crystal structure illustrations, in, Oak Ridge National Laboratory report ORNL-6895, Tennessee, 1996.
[33] J.-D. Chai, M. Head-Gordon, Long-range corrected hybrid density functionals with damped atom–atom dispersion corrections, Phys. Chem. Chem. Phys., 10 (2008) 6615-6620.
[34] B.P. Pritchard, D. Altarawy, B. Didier, T.D. Gibson, T.L. Windus, New basis set exchange: An open, up-to-date resource for the molecular sciences community, J. Chem. Inf. Model., 59 (2019) 4814-4820.
[35] M. Frisch, G. Trucks, H. Schlegel, G. Scuseria, M. Robb, J. Cheeseman, G. Scalmani, V. Barone, G. Petersson, H. Nakatsuji, Gaussian 16, in, Gaussian, Inc. Wallingford, CT, 2016.
[36] V. Barone, M. Cossi, Quantum calculation of molecular energies and energy gradients in solution by a conductor solvent model, J. Phys. Chem. A, 102 (1998) 1995-2001.
[37] T. Lu, F. Chen, Multiwfn: A multifunctional wavefunction analyzer, J. Comput. Chem., 33 (2012) 580-592.
[38] G. Zhurko, Chemcraft–graphical program for visualization of quantum chemistry computations, Ivanovo, Russia, 2005. https://chemcraftprog.com.
[39] L. Noodleman, Valence bond description of antiferromagnetic coupling in transition metal dimers, J. Chem. Phys., 74 (1981) 5737-5743.
[40] T. Mosmann, Rapid colorimetric assay for cellular growth and survival: Application to proliferation and cytotoxicity assays, J. Immunol. Methods, 65 (1983) 55-63.
[41] K. Yoshioka, H. Takahashi, T. Homma, M. Saito, K.-B. Oh, Y. Nemoto, H. Matsuoka, A novel fluorescent derivative of glucose applicable to the assessment of glucose uptake activity of *Escherichia coli*, Biochim. Biophys. Acta. Gen. Subj., 1289 (1996) 5-9.
[42] C. Zou, Y. Wang, Z. Shen, 2-NBDG as a fluorescent indicator for direct glucose uptake measurement, J. Biochem. Biophys. Methods, 64 (2005) 207-215.
[43] B.G. Tabachnick, L.S. Fidell. Experimental Designs using ANOVA. Belmont, CA: Duxbury Press, 2007.
[44] C. Marie, A.-M. Bralet, J. Bralet, Protective action of 1,3-butanediol in cerebral ischemia. A neurologic, histologic, and metabolic study, J. Cereb. Blood Flow & Metabolism, 7 (1987) 794-800.
[45] V.I. Bruyère, L.A.G. Rodenas, P.J. Morando, M.A. Blesa, Reduction of vanadium(V) by oxalic acid in aqueous acid solutions, Dalton Trans., (2001) 3593-3597.
[46] B. Baruah, V.O. Golub, C.J. O'Connor, A. Chakravorty, Synthesis of oxalato-bridged (oxo)vanadium(IV) dimers using L-ascorbic acid as oxalate precursor: Structure and magnetism of two systems, Eur. J. Inorg. Chem., 2003 (2003) 2299-2303.

[47] J. Salta, C.J. O'Connor, S. Li, J. Zubieta, Studies of the oxovanadium(IV)–oxalate system: syntheses and crystal structures of binuclear $(Ph_4P)_2[(VO)_2(H_2O)_2(C_2O_4)_3]\cdot 4H_2O$ and of the one-dimensional chain material, $(Ph_4P)[VOCl(C_2O_4)]$, Inorg. Chim. Acta, 250 (1996) 303-310.
[48] L.-M. Zheng, H.W. Schmalle, S. Ferlay, S. Decurtins, A Dinuclear vanadyl–oxalate compound, Acta Crystallogr., Sect. C: Crystal Struct. Commun., 54 (1998) 1435-1438.
[49] C. Chen, F.-Y. Bai, R. Zhang, G. Song, H. Shan, N. Xing, Y.-H. Xing, Synthesis, structure, and catalytic bromination of supramolecular oxovanadium complexes containing oxalate, J. Coord. Chem., 66 (2013) 671-688.
[50] S. Triki, F. Bérézovsky, J.S. Pala, M.-T. Garland, Synthesis and characterisation of new binuclear oxo-vanadium(IV) complexes with a bis(bidentate)oxalate bridge. Crystal structures of the cationic and anionic complexes $[V_2O_2(C_2O_4)(H_2O)_6]Cl_2\cdot 4Bu_4NCl\cdot H_2O$ and $[FeCp^*_2]_2[Et_4N]_2[V_2O_2(C_2O_4)(NCS)_6]$, Inorg. Chim. Acta, 308 (2000) 31-36.
[51] S. Yang, G. Li, S. Tian, F. Liao, J. Lin, Synthesis, structure, and magnetic properties of hydroxo-bridged vanadium oxalate $V_2O_2(OH)_2(C_2O_4)(H_2O)_2$, Eur. J. Inorg. Chem., 2006 (2006) 2850-2854.
[52] M.L. Tarlton, A.E. Anderson, M.P. Weberski Jr, X. Riart-Ferrer, B.M. Nelson, C.C. McLauchlan, Synthesis, characterization, and electrochemical properties of μ-oxalate bridged vanadium(III) and (IV) dimers incorporating the Kläui ligand, $CpP^{OR}Co$ (R= Me, Et), Inorg. Chim. Acta, 420 (2014) 159-165.
[53] L. Goerigk, N. Mehta, A trip to the density functional theory zoo: Warnings and recommendations for the user, Aust. J. Chem., 72 (2019) 563-573.
[54] C.F. Matta, R.J. Boyd, The Quantum Theory of Atoms in Molecules: From Solid State to DNA and drug design, first Ed., Wiley-VCH, (2007).
[55] W. Tang, E. Sanville, G. Henkelman, A grid-based Bader analysis algorithm without lattice bias, J. Phys: Condens. Matter, 21 (2009) 084204.
[56] M. Julve, M. Verdaguer, M.-F. Charlot, O. Kahn, R. Claude, Interactions in $Cu^{II}Cu^{II}$, $VO^{II}VO^{II}$ and $Cu^{II}VO^{II}$ pairs through oxalato bridging ligand, Inorg. Chim. Acta, 82 (1984) 5-12.
[57] R.L. Carlin, Magnetochemistry, Springer Science & Business Media, 2012.
[58] C.J. Ballhausen, H.B. Gray, The electronic structure of the vanadyl ion, Inorg. Chem., 1 (1962) 111-122.
[59] M.C. D'Antonio, M.M. Torres, D. Palacios, A.C. González-Baró, E.J. Baran, Vibrational spectra of the two hydrates of strontium oxalate, Spectrochim. Acta, Part A, 137 (2015) 486-489.
[60] K. Dewangan, N.N. Sinha, P.G. Chavan, P.K. Sharma, A.C. Pandey, M. More, D. Joag, N. Munichandraiah, N. Gajbhiye, Synthesis and characterization of self-assembled nanofiber-bundles of V_2O_5: Their electrochemical and field emission properties, Nanoscale, 4 (2012) 645-651.
[61] M. Malta, R.M. Torresi, Electrochemical and kinetic studies of lithium intercalation in composite nanofibers of vanadium oxide/polyaniline, Electrochim. Acta, 50 (2005) 5009-5014.
[62] N. Mancilla, M.C. D'Antonio, A.C. González-Baró, E.J. Baran, Vibrational spectra of lead(II) oxalate, J. Raman Spectrosc., 40 (2009) 2050-2052.
[63] Y. Chen, G. Yang, Z. Zhang, X. Yang, W. Hou, J.-J. Zhu, Polyaniline-intercalated layered vanadium oxide nanocomposites–one-pot hydrothermal synthesis and application in lithium battery, Nanoscale, 2 (2010) 2131-2138.
[64] E. Sánchez-Lara, A. Pérez-Benítez, S. Treviño, A. Mendoza, F. Meléndez, E. Sánchez-Mora, S. Bernès, E. González-Vergara, synthesis and 3D network architecture of 1- and

16-hydrated salts of 4-dimethylaminopyridinium decavanadate, $(DMAPH)_6[V_{10}O_{28}]\cdot nH_2O$, Crystals, 6 (2016) 65.
[65] F. Mabbs, Some aspects of the electron paramagnetic resonance spectroscopy of d-transition metal compounds, Chem. Soc. Rev., 22 (1993) 313-324.
[66] D. Mustafi, E.V. Galtseva, J. Krzystek, L.-C. Brunel, M.W. Makinen, High-frequency electron paramagnetic resonance studies of VO^{2+} in low-temperature glasses, J. Phys. Chem. A, 103 (1999) 11279-11286.
[67] R. Dulbecco, G. Freeman, Plaque production by the polyoma virus, Virology, 8 (1959) 396.
[68] A. Levina, A.I. McLeod, A. Pulte, J.B. Aitken, P.A. Lay, Biotransformations of antidiabetic vanadium prodrugs in mammalian cells and cell culture media: A XANES spectroscopic study, Inorg. Chem., 54 (2015) 6707-6718.
[69] Y.-L. Zhang, X.-S. Wang, W. Fang, X.-Y. Cai, H.-Z. Li, J.-W. Mao, X.-B. Jin, Y.-L. Bai, J.-Z. Lu, *In vitro* study of the cytotoxicities of two mixed-ligand oxovanadium complexes on human hepatoma cells, Pharmazie, 68 (2013) 827-834.
[70] H.B. Aliabad, S.K. Falahati-pour, H. Ahmadirad, M. Mohamadi, M.R. Hajizadeh, M. Mahmoodi, vanadium complex: An appropriate candidate for killing hepatocellular carcinoma cancerous cells, BioMetals, 31 (2018) 981-990.
[71] G. Vardatsikos, M.Z. Mehdi, A.K. Srivastava, Bis(maltolato)-oxovanadium(IV)-induced phosphorylation of PKB, GSK-3 and FOXO1 contributes to its glucoregulatory responses, Int. J. Mol. Med., 24 (2009) 303-309.
[72] M. Kongot, D.S. Reddy, V. Singh, R. Patel, N.K. Singhal, A. Kumar, Oxidovanadium(IV) and iron(III) complexes with O_2N_2 donor linkage as plausible antidiabetic candidates: Synthesis, structural characterizations, glucose uptake and model biological media studies, Appl. Organomet. Chem., 34 (2020) e5327.
[73] J. Ki, A. Mukherjee, S. Rangasamy, B. Purushothaman, J.M. Song, Insulin-mimetic and anti-inflammatory potential of a vanadyl-Schiff base complex for its application against diabetes, RSC adv., 6 (2016) 57530-57539.

Research Highlights

A highly water-soluble, oxalate-bridged binuclear oxidovanadium(IV) complex was synthesized in high yield by a simple and reproducible method > Spectroscopic and structural studies were performed in solution and in the solid state, and DFT calculations accessed the electronic structure of the product > The potential insulin-mimetic activity of **I** was demonstrated *in vitro* using the 2-NBDG uptake assay.

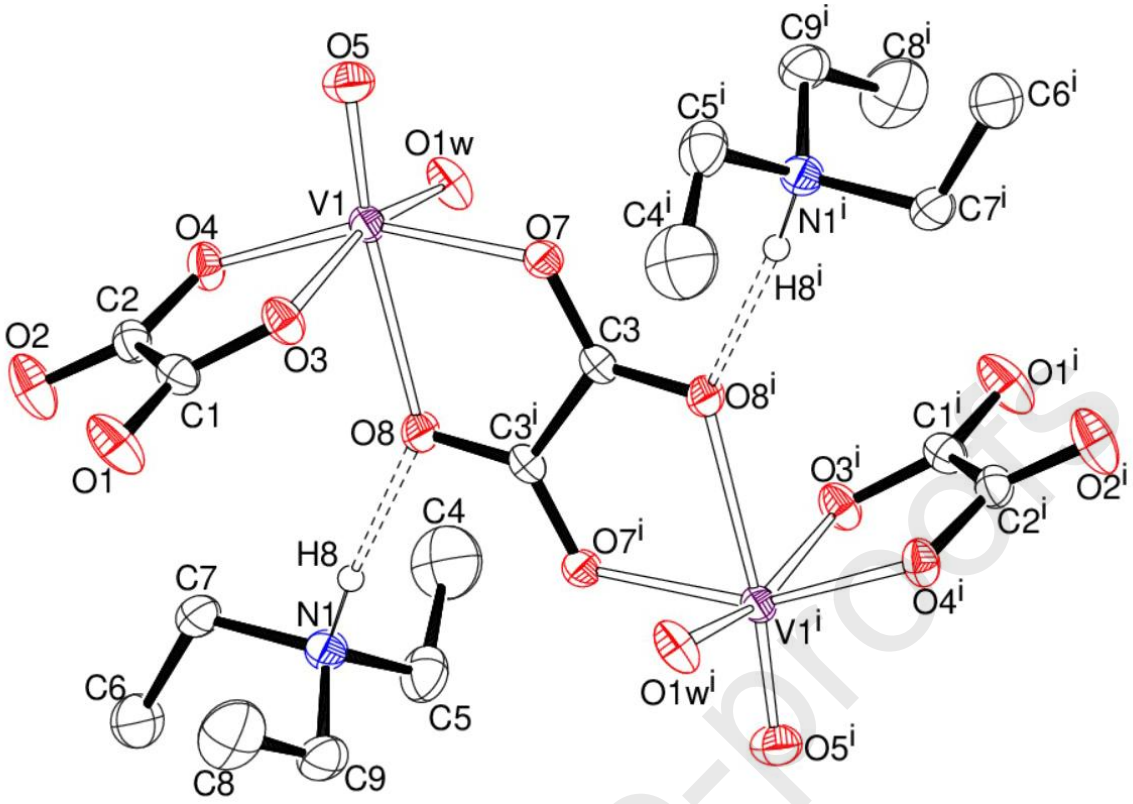

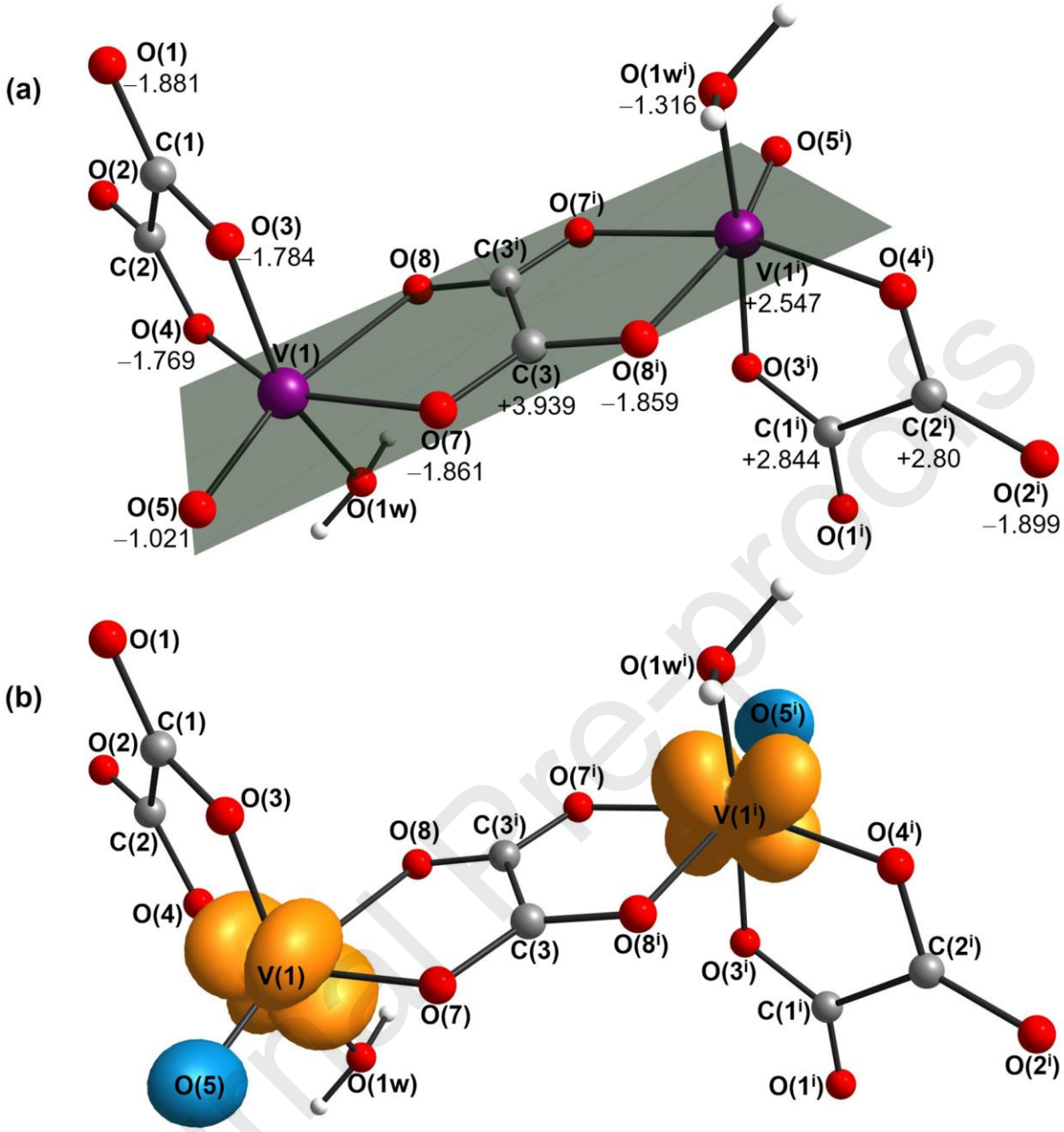

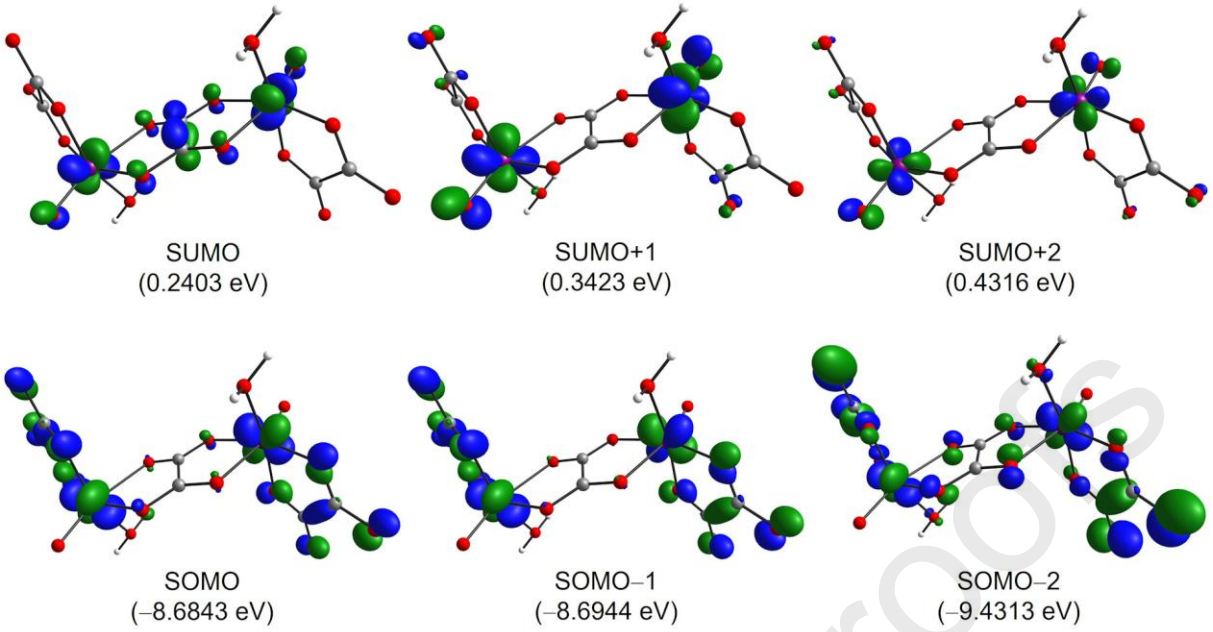

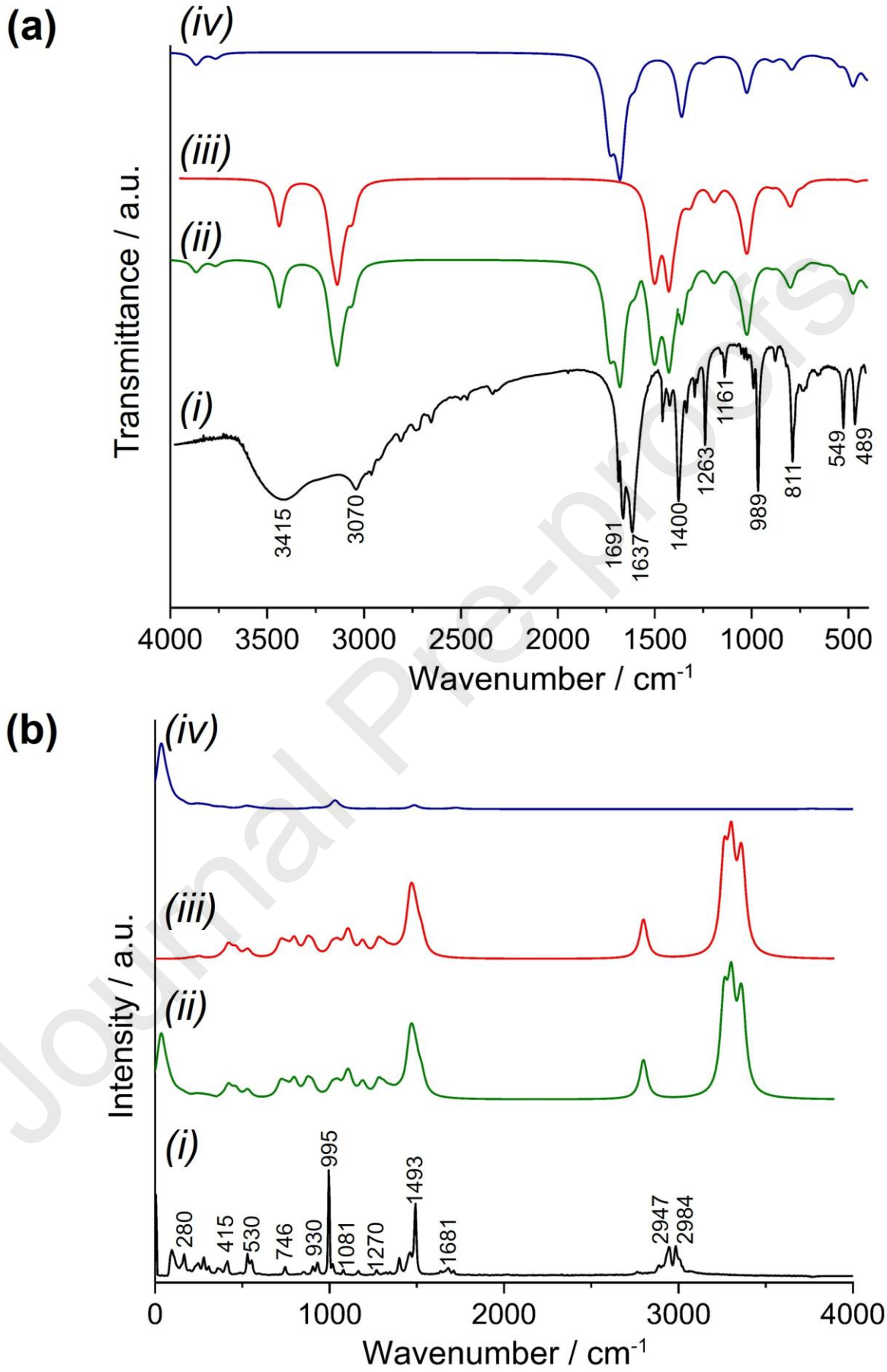

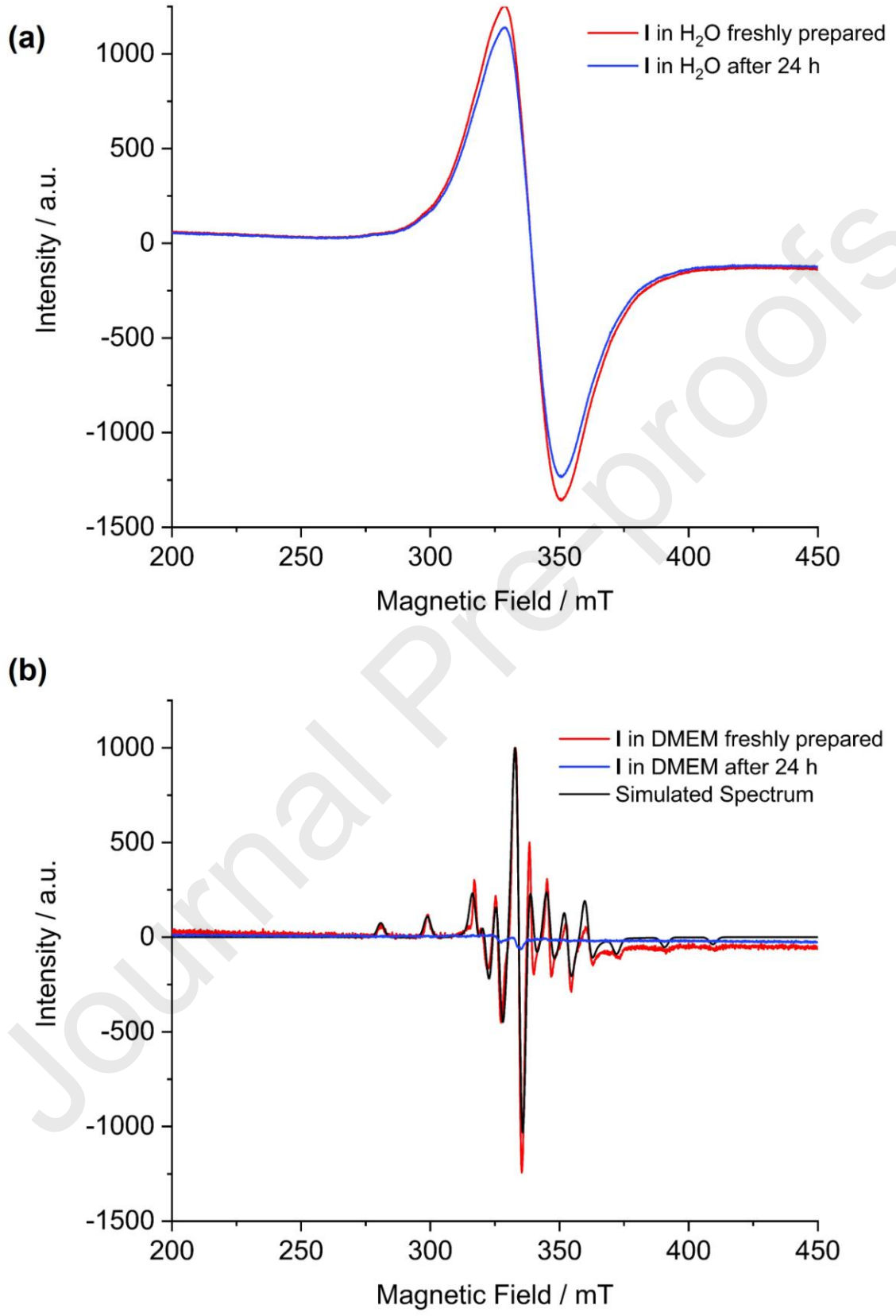

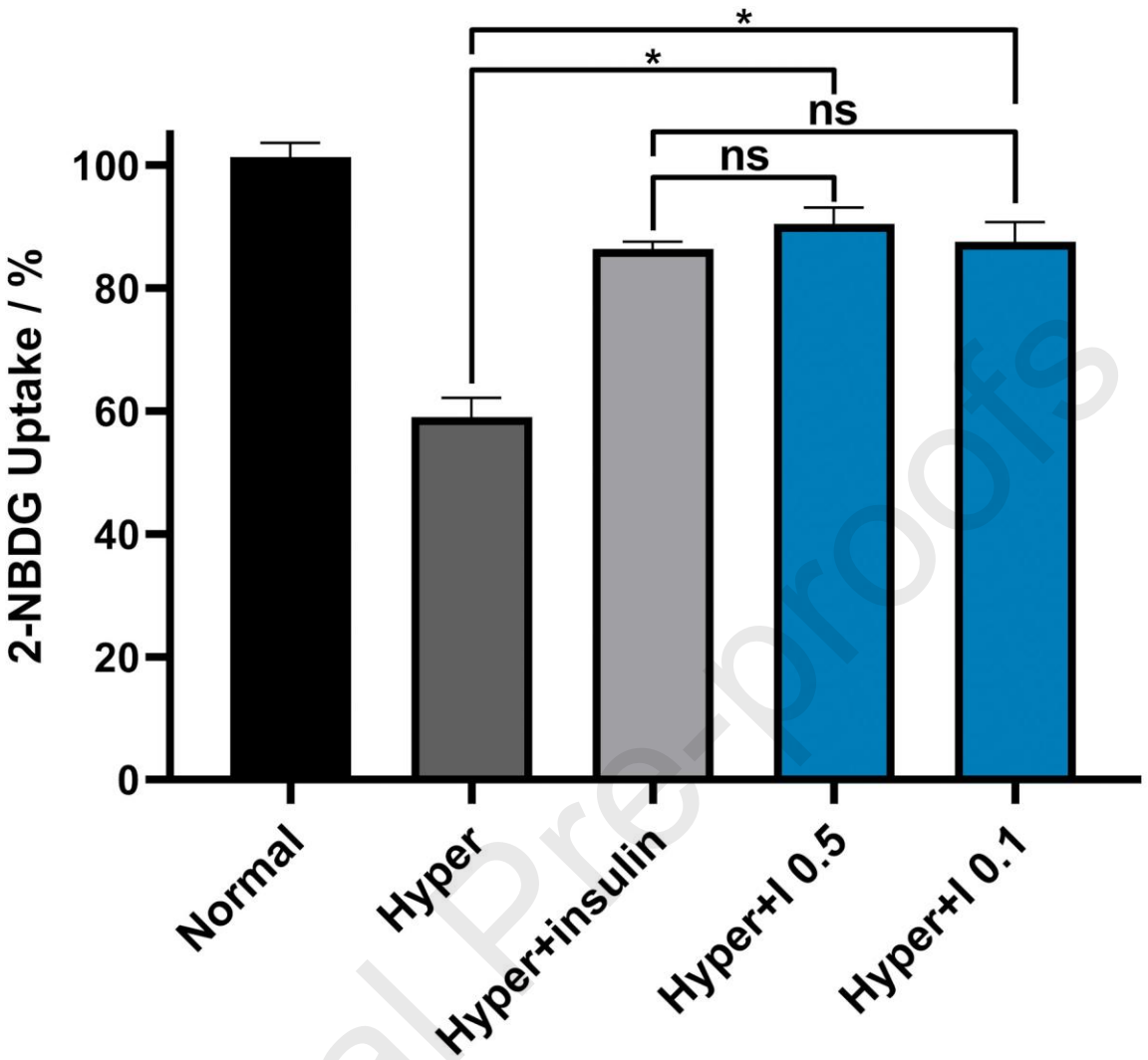

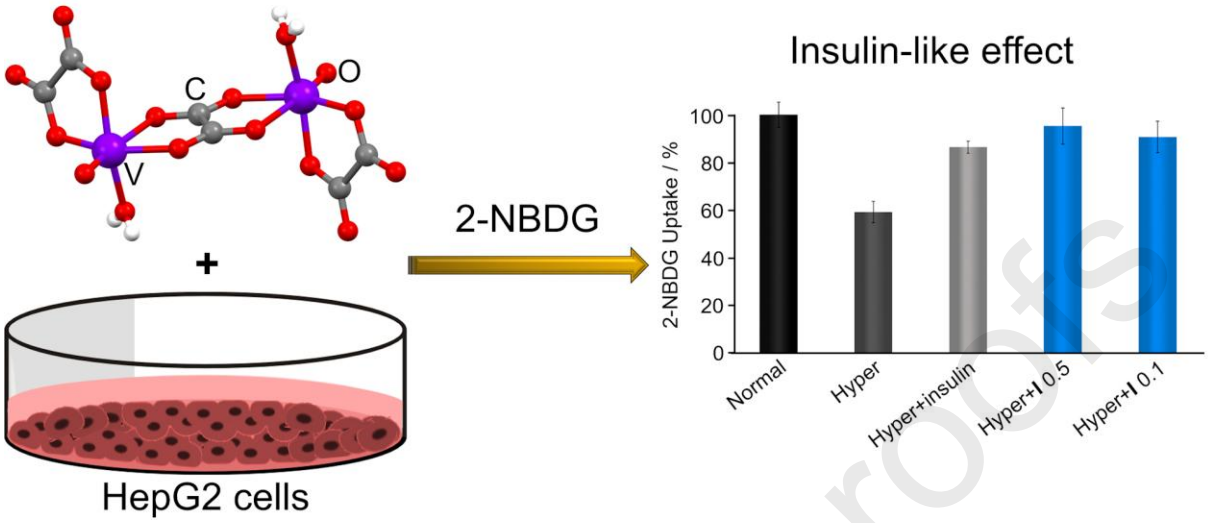

A highly water-soluble, binuclear oxalate-bridged oxidovanadium(IV) was synthesized, characterized, and studied by DFT method. Insulin-mimetic activity in hyperglycemic condition was evaluated *in vitro* using the 2-NBDG uptake by HepG2 cells. Finally, the chemical species present in aqueous solution and culture medium were investigated by EPR spectroscopy.